AD_____

Award Number:
W81XWH-10-2-0191

TITLE:
Biomedical Applications of Micro-Raman and Surface-Enhanced Raman Scattering (SERS) Technology

PRINCIPAL INVESTIGATOR:
Shiv K. Sharma, Ph. D.

CONTRACTING ORGANIZATION:
University of Hawaii Systems, Office of Research Services
Honolulu, HI 96822

REPORT DATE:
October 2012

TYPE OF REPORT:
REVISED FINAL

PREPARED FOR: U.S. Army Medical Research and Materiel Command
Fort Detrick, Maryland 21702-5012

REPORT DOCUMENTATION PAGE

Form Approved
OMB No. 0704-0188

1. REPORT DATE	2. REPORT TYPE	3. DATES COVERED
October -2012	Revised Final	30 September 2010-29 September 2012

4. TITLE AND SUBTITLE

Biomedical Applications of Micro-Raman and Surface-Enhanced Raman Scattering (SERS) Technology

5a. CONTRACT NUMBER

5b. GRANT NUMBER
W81XWH-10-2-0191

5c. PROGRAM ELEMENT NUMBER

6. AUTHOR(S)
Shiv K. Sharma, Anupam K. Misra, Ava C. Dykes, Lori E. Kamemoto,

E-Mail: shiv@hawaii.edu

5d. PROJECT NUMBER

5e. TASK NUMBER

5f. WORK UNIT NUMBER

7. PERFORMING ORGANIZATION NAME(S) AND ADDRESS(ES)

University of Hawaii Systems, Office of Research Services
Honolulu, HI 96822

8. PERFORMING ORGANIZATION REPORT NUMBER

9. SPONSORING / MONITORING AGENCY NAME(S) AND ADDRESS(ES)
U.S. Army Medical Research and Materiel Command
Fort Detrick, Maryland 21702-5012

10. SPONSOR/MONITOR'S ACRONYM(S)

11. SPONSOR/MONITOR'S REPORT NUMBER(S)

12. DISTRIBUTION / AVAILABILITY STATEMENT
Approved for Public Release; Distribution Unlimited

13. SUPPLEMENTARY NOTES

14. ABSTRACT
The purpose of this project was to evaluate Raman-based technologies for early detection of urogenital cancers. Most of the work was directed at improving different components of the surface-enhanced Raman scattering (SERS)-based immunoassay, analyzing tissue samples with micro-Raman imaging technology, micro-Raman and SERS detection of prostate cancer cells, and SERS detection of exfoliated cells from urine. The most significant findings were as follows. (i) The nitrocellulose membranes were proven to be an effective media for PSA capture. For SERS-based immunoassays, nitrocellulose offers comparable results to those obtained using gold-coated glass substrates while offering a more cost-effective and time-saving method of detecting minute amounts of PSA; (ii) Micro-Raman imaging technology was found to be effective in chemical mapping of arteries in the tissues of a *post mortem* individual whose cause of death was a cardiac event; (iii) Both micro-Raman and micro-SERS analysis were able to characterize the biochemistry at the molecular level of three types of prostate cancer cell lines (DU145, PC3 and LNCaP); and (iv) Micro-SERS analysis of exfoliated cells from the urine sample of a healthy volunteer showed the potential of the technique as the SERS spectra of individual cells could be measured with 1 s integration time, and various types of cells could be differentiated on the basis of their Raman spectra.

15. SUBJECT TERMS
Prostate cancer, PSA, micro-Raman spectroscopy, SERS, immunoassay, prostate cancer cells.

16. SECURITY CLASSIFICATION OF:			17. LIMITATION OF ABSTRACT	18. NUMBER OF PAGES	19a. NAME OF RESPONSIBLE PERSON
a. REPORT	b. ABSTRACT	c. THIS PAGE			USAMRMC
U	U	U	UU	68	19b. TELEPHONE NUMBER *(include area code)*

Table of Contents

Page

Introduction……..……..…… 4

Body…… 5
(i) SERS-Based Immunoassays for Detecting PSA ……. 8
(ii) Micro-Raman Imaging Technology for Chemical Mapping of Human Arteries……13
(iii) Micro-Raman and micro-SERS analysis of prostate cancer cell lines ……...21
(iv) Micro-SERS analysis of exfoliated cells from urine sample…….25

Key Research Accomplishments…….……..……..36

Reportable Outcomes……36

Conclusion ……36

References ……...37

Appendices ……..…40

INTRODUCTION

Recent advancements in Raman spectroscopy have made it an ideal method for the evaluation of biological samples[1-5]. Micro-Raman[4] and surface enhanced Raman scattering (SERS) spectroscopy[6-7] offer reduced sample volumes, increased spatial resolution, and increased sensitivity over conventional methods. In clinical applications these attributes can translate into less invasive sampling, smaller sample size, and earlier detection of target analytes. Raman technology[8] may enable earlier detection of urogenital cancers by extending the sensitivity and specificity of currently used serum- and urine-based clinical tests. Earlier detection of initial diagnosis as well as tumor recurrence could lead to improved patient prognoses and survival rates for these cancers.

A SERS-based immunoassay was proposed to evaluate serial blood samples from radical prostatectomy patients. By comparing these results to those obtained by conventional methods, more sensitive detection of prostate-specific antigen (PSA) could indicate prostate tumor recurrence earlier than other methods. Concurrently, tissue samples could be evaluated by micro-Raman spectroscopy to determine if spectral differences in normal and diseased tissue exist. If so, a new cancer detection method could be developed.

Until recently, Raman spectroscopy lacked the sensitivity needed for use as a readout method. Current advancements in surface-enhanced Raman scattering (SERS) detection have led to the incorporation of this technique into the immunoassay format. SERS is a surface sensitive occurrence that results up to 10^{14}-10^{15} enhancement of Raman scattering by analyte molecules adsorbed on the rough surfaces of coinage (Au, Ag, Cu) or alkali (Na, K, Li) metals.[9] SERS spectroscopy is thought to be the result of two contributing enhancement mechanisms, chemical and electromagnetic.[10] The chemical mechanism is associated with a charge transfer process between an adsorbed analytes and a metal surface. Essentially, the vibrations involved in the charge transfer process are enhanced, a phenomenon similar to resonant enhancement.[11] Enhancement produced by this component is in the 10-10^3 range.[9] The dominant electromagnetic contribution is due to an electromagnetic field enhancement caused by plasmon excitation through incident laser light on the metal surface. Electrons in the metal are excited to an oscillation in the metal cores, called a surface plasmon. Because the plasmon excitation is dependent on incident light, the excitation for a SERS experiment would ideally be adapted to the plasmon wavelength of the surface metal, which also affects the plasmon resonance wavelength.[11] The advantages of using SERS as a readout method versus fluorescence include the fact that Raman labels have narrow lines, which minimize the potential for spectral overlap when more than one label is involved. Secondly, Raman labels are not as prone as fluorescence to photobleaching at laser powers typically used for sample evaluation, allowing for greater signal-to-noise ratios through longer collection times. Lastly, there are fewer limitations concerning the excitation wavelength for Raman labels. Raman spectra are molecule specific. The narrow Raman bands are recorded as Raman shifts (in cm^{-1}) with respect to the excitation wavelength and Raman spectral features do not change with changing excitation wavelength. Additionally, spectra from multiple Raman labels excited by a single wavelength could be interpreted with less difficulty than the emission of multiple fluorophores in most instances.[12]

Grubisha *et al.*[13] have successfully utilized SERS with a sandwich immunoassay for detecting PSA. They employed monoclonal antibodies for prostate-specific antigen (PSA) coupled to

Raman reporter-coated gold nanoparticles (AuNPs); the PSA could be detected in a serum matrix down to 1 pg/ml. The Raman peak resulting from the symmetric nitro stretch of the bifunctional reporter 5, 5'-dithiobis (succinimidyl-2-nitrobenzoate) (DSNB) was monitored while measuring samples containing a range of concentrations of PSA. While a limit of detection (LOD) of 1 pg/ml is well within the normal limits of PSA levels in a normal healthy male, the ability to monitor even lower levels may prove beneficial in following prostate cancer patients.

In the United States, prostate cancer is the second leading cause of cancer deaths in men.[14] There is currently no cure for locally advanced or metastatic prostate cancer; early detection and treatment are essential for a favorable prognosis. PSA is a serine protease whose functions in the seminal fluid are the liquefaction of semen and the dissolution of the cervical mucus cap, which allows for the entry of sperm into the cervix for fertilization. PSA is released into the blood of healthy males at low concentrations. In males afflicted with prostate cancer, PSA levels are increased and can be correlated with tumor volume and tissue specificity. Although routine PSA screenings have resulted in 90% of all prostate cancers being diagnosed at an early, treatable stage[15], the PSA assay finds its greatest utility as a prognostic indicator of prostate cancer recurrence. Studies have shown that serial evaluation of PSA levels post-prostate cancer treatment is effective in identifying recurrence or further metastasis.[16]

Another laboratory test where SERS can be a useful readout method is a variation of the immunoassay called the dot blot.[17-19] Traditionally a dot blot is a colorimetric method where the detection of these proteins is accomplished through the application of assorted dyes followed by their measurement via a densitometer.[20] A convenient and timesaving method, dot blotting involves the spotting of a protein onto an immobilizing matrix, such as nitrocellulose (NC) or a polyvinylidene fluoride (PVDF) membrane. We found that for detection via SERS spectroscopy NC is the matrix of choice because it offers low background, minimal preparation prior to protein application, and optimal position of Raman bands. Furthermore, it does not require any additional sample preparation and offers increased sensitivity to other detection methods. Depending on the dye used for visualization, dot blots analyzed by optical methods have limits of detection in the nanogram range, however, some are as low as 20 pg/ml.[16,17,21] The use of the dot blot method for detecting PSA by SERS spectroscopy has been demonstrated down to a concentration of 100 fg/ml.[22]

BODY

During the two years of the research project, we proposed to undertake the following tasks under this contract W81XWH-10-2-0191.

Year 1

Task 1. Establish the Raman Biomedical Research Program at the University of Hawaii in collaboration with Tripler Army Medical Center. These facilities will further the biomedical and clinical applications of Raman techniques for the investigation of health disparities of importance to the armed forces. (Month 1 to 3) and submit first quarterly report **100% Complete**

Task 2. Initiate interdisciplinary collaborative research between physicists and clinicians towards improving medical care through Raman technology. (Month 1 to 6) **100% Complete**

Task 3. Obtain approval from the University of Hawaii Committee on Human Studies. (Month 1 to 3) **100% Complete**

Task 4. Obtain approval from the TAMC Institutional Review Board. (Month 1 to 6) **100% Complete**

Task 5. Obtain approval from USAMRMC ORP. (Month 1 to 6) **75% Complete**

Task 6. Begin recruitment of participants who have undergone radical prostatectomy for PSA study. (Month 3 to 6) **0% Complete**

Task 7. Receive perishable laboratory supplies needed for SERS and micro-Raman techniques. (Month 3 to 6) **100% Complete**

Task 8. Prepare non-perishable components of micro-Raman and SERS assays. (Month 3 to 6), and prepare second quarterly report **100% Complete**

Task 9. Prepare and test microcavity substrate component of immunoassay (Months 3 to 6) **100% completed**

Task 10. Begin sample collection from PSA study participants. (Month 6 to 9) **0% Complete**

Task 11. Begin to measure serum PSA levels in sera from post-prostatectomy patients using ultrasensitive SERS techniques. (Month 6 to 9) and prepared third quarterly report. (**0% of competed for sera from patients**, **25% Complete for Lab-based SERS PSA testing**)

Task 12. Begin data analysis of spectra obtained from SERS immunoassays. (Month 6 to 12) **0% Complete**

Task 13. Continue to monitor serum PSA levels using SERS techniques. (Month 9 to 12) **0% Complete**

Task 14. Develop mechanism to obtain flash-frozen urogenital tract tissue samples for Raman spectroscopy, including IRB approval. (Month 9 to 12) **0% Complete**

Task 15. Begin RCC participant recruitment. (Month 9 to 12) **0% Complete**

Task 16. Complete and submit all necessary reporting requirements (e.g., quarterly progress reports, annual report). (Month 9 to 12) (**Completed Reporting Requirements**) **100% Complete**

Year 2

Task 1. Continue to monitor serum PSA levels in post-prostatectomy patients via SERS methods over the two year period to determine correlation with tumor recurrence. (Month 13 to 24) **0% Complete**

Task 2. Examine urogenital tract cancer tissue samples with micro-Raman techniques, which may lead to better surgical delineation of tumor vs. normal tissue, new detection methods, and other clinical applications. (Month 13 to 18), and prepare 5th quarterly report. **50% Complete**

Task 3. Begin collecting urine samples from RCC participants. (Month 13 to 18) and prepare 6th quarterly report. **50% Complete**

Task 4. Begin micro-Raman and SERS examination of exfoliated normal and cancer cells from urine. (Month 15 to 24), and prepare 7th quarterly report. 5**0% Complete**

Task 5. Refine feasible micro-Raman and SERS methods for cell and tissue examination. (Month 18 to 24) 75**% Complete**

Task 6. Submit papers for peer-reviewed publications and presentations based on our findings. (Month 21 to 24) Submitted manuscript on applications of micro-Raman for analyzing 5**0% Complete**

Task 7. Complete and submit all necessary reporting requirements. (e.g., quarterly progress reports, annual report, and final report). (Month 21 to 24) **100% Complete.**

We established the Biomedical Raman Center at the University of Hawaii in an informal collaboration with Tripler Army Medical Center's clinicians to further the clinical application of Raman techniques. We obtained initial approval for the proposed work from University of Hawaii (UH) Committee on Human Studies on October 20, 2010 (see Appendix I(a)). We received continual annual approval for undertaking the proposed work under this contract from the UH Committee on Human Studies on August 26, 2011, and on July 19, 2012 to expire on July 17, 2013 (see Appendix I (b) and (c)).

On August 12, 2011, a letter of support for the program was provided to Dr. Jeffrey L. Berenberg, surgeon at Tripler Army Medical Center, by the Director of the Hawaii Institute of Geophysics and Planetology, University of Hawaii (see Appendix II). The letter committed the use of UH facilities to further the biomedical and clinical application of Raman techniques for the investigation of health disparities of importance to the armed forces. While this informal collaboration is well established, Tripler Army Medical Center initiated a CRADA with UH to formalize the entity. Unfortunately it took a long time to get the paper work approved by various administrative authorities. On October 14, 2012, we were informed by Dr. Berenberg that the protocol for Biomedical Applications of Micro-Raman and Surface-Enhanced Raman Scattering (SERS) Technology was officially approved but we were not approved to initiate any CRADA related research activities until Dr. Berenberg received a separate CRADA approval (see Appendix III). The clinical sample tasks listed on pages 5 and 6 remain incomplete as we did not have access to these samples.

The current contract ended on Oct. 29, 2012. We decided to close the contract and not seek a NO COST Extension partly because of delay in paper work in getting approvals for the clinical samples and more importantly because of the loss of key personnel at UH for this project as Dr. Ava Dykes left UH and accepted a job in West Virginia.

Much of work during this contract was directed at improving different components of the SERS-based immunoassay, analyzing tissue samples with micro-Raman imaging technology, micro-Raman and SERS detection of prostate cancer cells, and SERS detection of exfoliated cells from urine. Our most significant findings are as follows. (i) The nitrocellulose membrane was proven to be an effective medium for PSA capture. For SERS-based immunoassays, nitrocellulose

offers comparable results to those obtained using gold-coated glass substrates while offering a more cost-effective and time-saving method of detecting minute amounts of PSA. (ii) Micro-Raman imaging technology has been found to be effective in chemical mapping of arteries in the tissues of a *post mortem* individual whose cause of death was a cardiac event. (iii) Both micro-Raman and micro-SERS analysis were able to characterize the biochemistry at the molecular level of three types of prostate cancer cell lines (DU145, PC3 and LNCaP). (iv) Micro-SERS analysis of exfoliated cells from urine sample of a healthy volunteer showed the potential of the technique as the SERS spectra of individual cells can be measured with 1 s integration time, and various types of cells can be differentiated on the basis of their spectra. We briefly outline the key achievements in the following pages.

(i) SERS-Based Immunoassays for Detecting PSA

Following is a brief description of the SERS Immunoassays for detecting PSA that was developed with partial support from this contract. Some of these results have appeared in the manuscript entitled "Nitrocellulose-based SERS Immunosensor for Detection of Biological Molecules" published in the "*Proceedings of Smart Biomedical and Physiological Sensor Technology VIII* (2011)" (See Appendix IV). The following is a summary of this work on SERS-based immunoassays sensor of PSA.

METHODOLOGY

Antibodies to PSA were purchased from Fitzgerald Industries (Concord, MA, USA), and the PSA antigen was purchased from Bios Pacific (Emeryville, CA, USA). We also tested two different anti-PSA antibodies, i.e., mouse monoclonal [5A6] and [5G6] anti-PSA antibodies. ImmunoPure normal human serum was acquired from Pierce Biotechnology (Rockford, IL, USA). Unless otherwise stated, all other reagents were used as received from Sigma Aldrich (St. Louis, MO, USA).

Gold nanoparticle (AuNP) preparation

Gold colloids were made by adding 1 ml of 1% hydrogen tetrachloroaurate (III) ($HAuCl_4$) to 100 ml of distilled water, followed by 2 ml of 1% sodium citrate tribasic dihydrate ($Na_3C_6H_5O_7$). Approximately 1 ml of 0.1M K_2CO_3 was added to adjust the pH to 7.16. The solution was heated under reflux for 20 to 30 minutes, until the color turned a deep purple. Evaluation by photon correlation spectroscopy revealed that particle size was approximately 20 nm. The concentration of AuNPs in the solution was calculated to be 9.23×10^{11} particles/ml.

DSNB (5,5′-dithiobis (succinimidyl-2-nitrobenzoate)) synthesis

Synthesis of DSNB was carried out as previously described.[13] Briefly, 0.50 g of 5, 5′-dithiobis (2-nitrobenzoic acid) (DNBA), 0.52 g of 1, 3-dicyclohexylcarbodiimide (DCCD), and 0.29 g of *N*-hydroxysuccinimide (NHS) were sequentially added to 50 ml tetrahydrofuran in a 500 ml round-bottom flask equipped with a drying tube. After stirring for 24 hours at room temperature, the solution was filtered and then rotoevaporated to remove the solvent. The product was then recrystallized as a yellow powder with acetone/hexane solvent.

Preparation of DSNB-labeled immunogold colloids

DSNB-labeled SERS reporters were made by adding 100 µl of 2.5mM DSNB in acetonitrile to 1 ml of unconjugated gold sol and allowing the reaction to proceed for 4 to 8 hours. The mixture was then centrifuged at 10,000 g for 7 minutes. The clear supernatant was discarded and the loose sediment was resuspended in 1 ml borate buffer (2 mM, pH 9). Next, 35 µg of detection antibody (14.3 µl of a 2.45 mg/ml PSA-66 solution) was added. This mixture was incubated at room temperature for 1 hour. After a second centrifugation and removal of the supernatant, the precipitate was resuspended in 1 ml of 2 mM Tris buffer (pH 7.6) with 1% bovine serum albumin (BSA).

Figure 1(A) demonstrates the basic reaction between DSNB and a single gold nanoparticle. The interaction of DSNB with the gold surface results in AuNP coated with a thiolate of DSNB. The intermediate species formed is a Raman reporter-labeled AuNP containing a reactive group, $R(C_5H_5NO_3)$. This Raman reporter molecule can then react with the primary amine of an antibody by forming an amide linkage[13], thus creating a bifunctional Raman reporter. Figure 1(B) depicts how multiple reporters may interact with a single AuNP. The presence of the reactive groups allow for the coupling of the antibody at the distal end of the reporter. Monofunctional reporters position antibodies alongside the reporters where they compete for available space. A monofunctional reporter such as this would accommodate fewer antibody molecules, allowing for the attachment of fewer antigens. Additionally, the monofunctional configuration would permit a smaller number of reporters per AuNP, resulting in a decreased signal from each reporter construct.

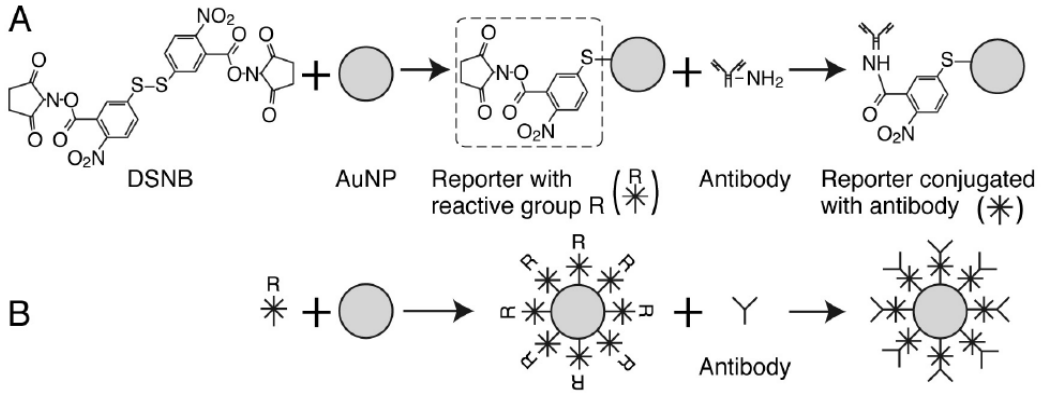

Figure 1. (A) Conjugation chemistry of DSNB molecule with AuNPs. Exposure of DSNB to the gold surface yields an AuNP coated with the thiolate of DSNB. The thiolate contains a reactive group that then forms an amide linkage with the primary amine of an antibody. **(B)** Schematic representation of AuNP-antibody orientation following reaction with DSNB. The bifunctional nature of this reporter allows for a greater number of reporters to be associated with each AuNP and a matching number of antibodies can, in turn, be associated with each reporter.

Preparation of modified dot blot

A 3×4 grid was drawn on a 3″×3″ square of nitrocellulose membrane using a pencil. We then diluted 5 µl of PSA in phosphate-buffered saline (PBS, pH 7.5) ranging from concentrations of 0 to 10 µg, which were pipetted to the center of each square. After drying, the membrane was pre-wet with a solution of 0.5% Tween 20 in phosphate-buffered saline (PBS-T). The SNAP i.d.

protein detection system (Millipore Corporation, Billerica, MA) was used for blocking and antibody introduction to the membrane. After placing the membrane in the blot holder, it was positioned in the SNAP i.d. system. Thirty milliliters of SuperBlock T20 blocking buffer were poured into the blot holder and allowed to incubate for 10 minutes. A vacuum was applied to system until the blot holder well was completely empty. Next, 3 ml of the anti-PSA-DSNB-labeled gold nanoparticles were placed in the well and allowed to incubate for 10 minutes. The vacuum was applied to pull the antibody solution through the membrane then left on during three consecutive rinses with PBS-T. The blot was removed from the holder and allowed to air dry. It was then affixed to an aluminum block with double-sided tape in preparation for evaluation with micro-Raman spectroscopy.

UV-visible spectroscopy

UV-visible spectroscopy scans were conducted using an Evolution 60 spectrophotometer (Thermo Scientific, Madison, WI, USA) equipped with a xenon light source. Gold nanoparticles were evaluated by scanning 450 to 1000 nm in absorbance mode with a wavelength interval of 1 nm.

Micro-Raman spectroscopy

All SERS spectra were excited by an Invictus 785-nm NIR laser and measured with a fiber-coupled micro-Raman RXN system (Kaiser Optical Systems, Inc., Ann Arbor, MI) equipped with a 50-micron slit. The micro-Raman system uses a 785 nm CW laser and CCD detector. A 10× objective (NA 0.25) that produced a 75 μm laser spot size on the sample was used for all measurements. The Rayleigh scattered laser radiation was rejected by utilizing a 785 nm notch filter. The cosmic rays were removed using software provided by Kaiser optical system, which measures the spectra twice and deletes the random peaks due to cosmic rays.

RESULTS AND DISCUSSION

Evaluation of SERS activity of AuNPs

Figure 2 shows the absorbance spectra for a series of AuNP solutions of differing pH values prepared under otherwise identical conditions in our laboratory. Only those AuNPs prepared at pH 7.0 display a large absorbance in the NIR region. The deep purple hue of our AuNP preparation correlates with this finding and is proof of aggregate formation.[23] Rather than the red color, which is characteristic of a single particle plasmon region, this Au solution more strongly absorbs and scatters light over a broad band of longer wavelengths and appears purple.[24]

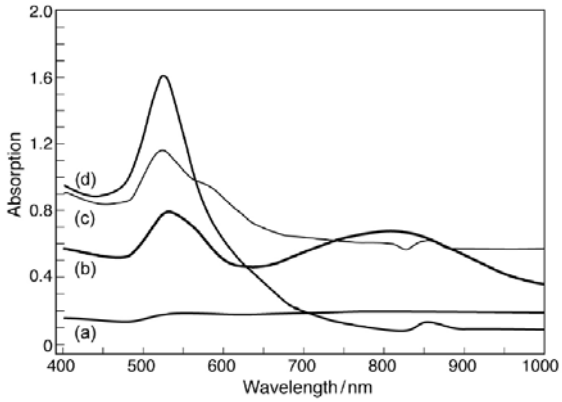

Figure 2. Absorbance spectra of gold sols prepared at a range of pH values: (a) pH 6.0; (b) pH 7.0; (c) pH 8.0; and (d) pH 9.0. Spectral curves have been displaced vertically for clarity.

SERS-based prostate specific antigen sensor

As discussed above, the anti-PSA-DSBN-AuNPs were used in the assembly of a PSA dot blot assay. Figure 3 shows the resultant SERS spectra of the Raman reporter molecule DSNB for PSA concentrations from 100 fg/ml to 10^6 fg/ml.

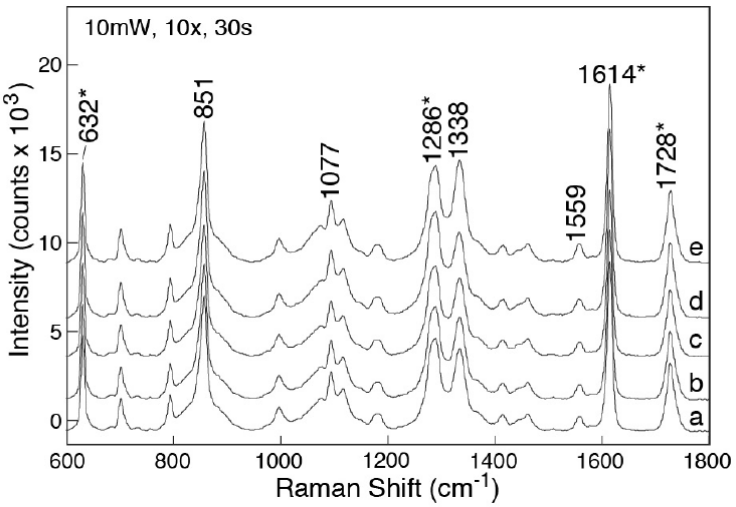

Figure 3. SERS spectra of PSA dot blot assay acquired at PSA concentrations of (a) 10^2, (b) 10^3, (c) 10^4, (d) 10^5, and (e) 10^6 fg/ml, respectively. Each spectrum was measured with 10 mW of laser power and 30 s integration time. The bands due to nitrocellulose membrane are marked by asterisks (*).

A plot of the intensity of the peak at 1338 cm^{-1} yields the graph in Figure 4. Each point represents the average of the intensity of this peak from ten different spectra. Note PSA concentrations of 10^3, 10^6, and 10^9 fg/ml correspond to 1 pg/ml, 1 ng/ml, and 1 μg/ml, respectively. Because the intensities associated with 1 and 10 fg/ml concentrations were not significantly different from zero, the LOD for this assay was found to be 100 fg/ml.

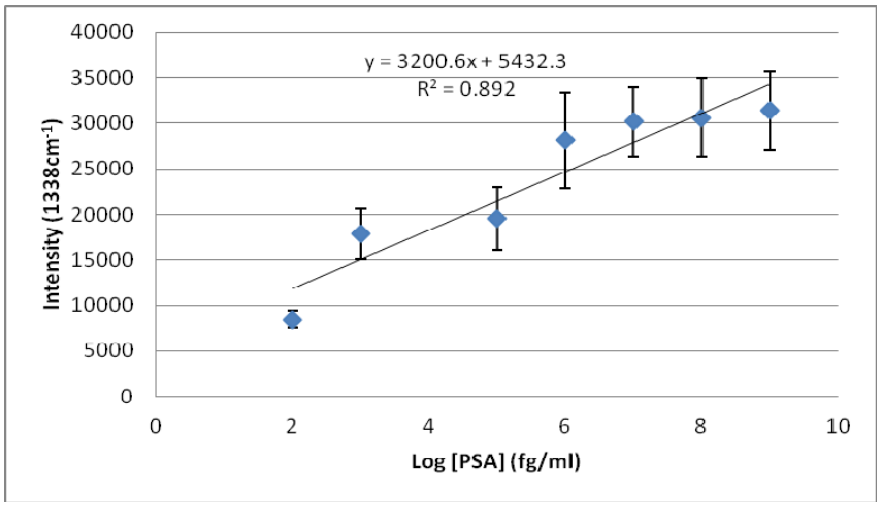

Figure 4. Results of SERS-based PSA immunoassay using monoclonal anti-PSA [5A6].

Mouse monoclonal [5G6] to PSA is an IgG1 isotype antibody. The results of a SERS-based PSA immunoassay using this antibody are shown in Fig. 5. The PSA was detected down to 1 pg/ml with and improved R^2 value of 0.986. These results show that either antibody is suitable for use in the SERS immunoassay. The increased sensitivity when using the 5A6 antibody shows great promise. The reduced variability associated with the improved coefficient of variability (R^2) of the 5G6 assay is also a desirable characteristic. This antibody may also be used in cases where sensitivity below 1pg/ml is not crucial.

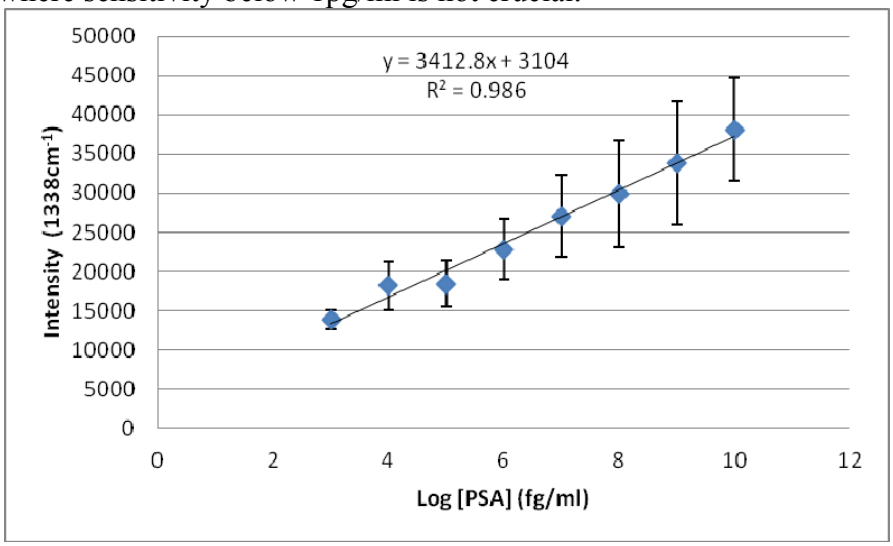

Figure 5. Results of SERS-based PSA immunoassay using mouse monoclonal anti-PSA [5G6].

The PSA assays currently in clinical use are typically a double monoclonal antibody sandwich reaction with electrochemiluminescent or fluorescent detection. These technologies have a sensitivity of about 0.1ng/ml. Lower values typically cannot be distinguished from zero and are reported as < 0.1ng/ml.[16] Although this LOD is adequate for an initial evaluation for the

presence of prostate cancer (PC), patients who have been treated for PC by undergoing radical prostatectomy (RP) will have very low to zero PSA in their blood. Monitoring PSA levels with lower LOD in these patients can be effective in identifying recurrence or further metastasis earlier than previously possible.[16] Because PSA elevations in serum occur earlier than the development of clinical symptoms, PSA-defined biochemical relapse is now widely accepted as an early indicator of tumor recurrence.[26] The development of detection methods such as the SERS-based immunoassay that are capable of measuring PSA below the current detectable limit could lead to earlier detection and treatment of recurrent prostate cancer, enabling earlier relapse detection and intervention.

(ii) Micro-Raman Imaging Technology for Chemical Mapping of Human Arteries

To demonstrate the versatility of our SERS detection method with micro-Raman spectrometer, antibody-DSNB-AuNP substrates were constructed using antibodies to proteins found in human arteries containing vulnerable plaques. Human femoral arteries were obtained *post mortem* from an individual whose cause of death was a cardiac event. The samples were transported from John A. Burns School of Medicine by Professor John S. Allen of Mechanical Engineering under the approved UH Biosafety Program. The results of this investigation have been published in a manuscript, "*In vitro* quantitation of human femoral artery atherosclerosis using near-infrared Raman spectroscopy" that appeared in the *Proceedings of Smart Biomedical and Physiological Sensor Technology IX* (2012) (see Appendix V for a copy of the reprint). The following is a summary of this work that indicates that Raman mapping, respectively, with 961 and 1073 cm^{-1} can allow precise location of the calcified plaque boundaries containing calcium hydroxyapatite and carbonate apatite, respectively.

Atherosclerosis is a systemic disease in which fatty deposits, inflammation, cells, and scar tissue build up within artery walls. In advanced lesions these deposits accumulate, followed by the formation of calcium containing crystals. This ultimately leads to calcification of the artery wall.[27] Atherosclerosis now accounts for nearly three-fourths of all deaths from cardiovascular disease and is the underlying cause of the majority of clinical cardiovascular events such as heart attack and stroke.[28] Both coronary artery disease (CAD) and peripheral artery disease (PAD) are clinical manifestations of atherosclerosis. However, patients diagnosed with atherosclerosis tend to develop the disease in different types of arteries. Approximately 60% of patients with severe PAD requiring surgery were found to have significant CAD in at least one vessel.[29] In fact, PAD is known to be a marker for systemic atherosclerosis.[28] For this reason, it is important to study atherosclerosis in vessels of the extremities. The femoral artery is of particular interest because 72% of all occlusions occurring in the leg originate in the femoral artery within the adductor canal.[30]

In the majority of cases, atherosclerosis is not detected until it becomes symptomatic, such as when significant stenosis or occlusion occurs. However, asymptomatic or noncritical stenoses are also clinically relevant. The rupture of non-occlusive plaques followed by rapid plaque enlargement is the most important mechanism for acute coronary syndromes such as myocardial infarction and crescendo angina.[31] Recent studies support the theory that plaque composition rather than size or volume determines whether a lesion will rupture and could lead to a cardiac event.[32] Current technology offers only limited information about plaque composition.

Intravascular ultrasound yields mainly morphological information. Magnetic resonance imaging (MRI) can detect large lipid pools and calcifications but cannot quantify the chemical composition of these areas. Directional coronary atherectomy provides histological information but is a destructive technique and only detects advanced lesions.[32] Autofluorescence showed some promise as a laser angioplasty guidance system due to the inherent fluorescence of vessel wall and atherosclerotic plaque constituents, but this method offers little biochemical information.[33] For these reasons Raman spectroscopy has become an ideal candidate for the detection of early atherosclerosis. Raman techniques are noninvasive, nondestructive, and can reveal the chemical composition of the target tissue. The use of near-infrared Raman spectroscopy eliminates interference from inherent autofluorescence.

METHODOLOGY

Human Artery Samples

Human femoral arteries were obtained *post mortem* from an individual whose cause of death was a cardiac event. Artery segments were frozen at -30°C until sectioning. Ten micron sections were captured on 1"x3" slides cut from commercially available polished aluminum sheets with a thickness of 0.5 mm (Anomet, Inc., Ontario, Canada). Sections mounted on aluminum slides were stored at -80°C. The slides were warmed to room temperature before examination by Raman spectroscopy.

Artery sections interrogated by SERS immunohistochemistry required further preparation. Ten micron sections of human femoral artery mounted on aluminum slides were fixed and permeated by exposure to ice-cold methanol for 5 minutes. After rinsing three times with phosphate-buffered saline (PBS), the arteries were blocked using 5% bovine serum albumin (BSA) in PBS for 1 hour. The sections were again rinsed three times with PBS before treatment with an antibody- DSNB-AuNP reporter as described below. The arteries were next exposed to either anti-von Willebrand factor (vWF)-DSNB-AuNP or anti-Ki67-DSNB-AuNP reporters for 1 hour at room temperature. The slides were then rinsed three times in PBS and allowed to air dry before study.

DSNB-labeled SERS reporters were constructed as previously described.[22] In brief, reporters were made by adding 100 μl of 2.5 mM DSNB in acetonitrile to 1ml of unconjugated gold sol. The resulting reaction was allowed to proceed for 4 to 8 hours. The mixture was then centrifuged at 10,000 g for 7 minutes. The clear supernatant was discarded and the loose sediment resuspended in 1 ml of a borate buffer (2 mM, pH 9). Next, 35 μg of detection antibody was added. The detection antibodies used here included rabbit polyclonals to either von Willebrand Factor (vWF) or Ki67 (Abcam, Inc. Cambridge, MA). This mixture was incubated at room temperature for 1 hour. After a second centrifugation and removal of the supernatant, the precipitate was resuspended in 1 ml of 2 mM Tris buffer (pH 7.6) with 1% BSA.

Micro-Raman spectroscopy

All spectra were excited by an Invictus 785-nm NIR laser and measured with a fiber-coupled micro-Raman RXN system (Kaiser Optical Systems, Inc., Arbor, MI) equipped with a 50 micron slit. The micro-Raman system uses a 785 nm CW laser and CCD detector. A 50× objective that

produced a 5 μm laser spot size on the sample was used for all measurements. The Rayleigh scattered laser line is rejected by utilizing a 785 nm notch filter. The cosmic rays were removed by the software provided by Kaiser optical system, which measures the spectra twice and deletes the random peaks due to cosmic rays. The spectra were collected with 10 mW of laser power at the sample and 120 s of integration time.

Chemical mapping was used to evaluate human femoral arteries. A 10x10 matrix of points was selected for Raman sampling for a total of 100 spectra from each area. We identified areas containing calcified plaques by mapping the intensity of peaks 961 and 1073cm^{-1}. We also identified areas containing high amounts of cholesterol by mapping the intensity of the peak at 1442cm^{-1}.

SERS spectra were also obtained with the fiber-coupled micro-Raman RXN system (Kaiser Optical Systems, Inc., Arbor, MI). These spectra were collected with 10 mW of laser power at the sample and 60 s of integration time.

RESULTS AND DISCUSSION

Representative micro-Raman spectra of human femoral arteries are shown in Figs. 6 and 7. Raman spectra from sections of artery containing calcified plaques are known to be two- to five-fold higher in intensity than normal areas.[27] Peaks associated with cholesterol also have higher intensity, reflecting a higher concentration of the material in these areas. The peaks at 1442 cm^{-1} and the area from 2800 to 3000 cm^{-1} are most obviously affected. The presence of peaks that are unique to the calcified plaque areas is also notable. Strong peaks at 961 and 1073 cm^{-1} are due to phosphate and carbonate symmetric stretching in calcium hydroxyapatite and carbonate apatite, respectively.

Other noted peaks are listed in Table 1. Peaks associated with the aromatic ring in the amino acid phenylalanine are located at 1004 and 1037 cm^{-1}.[34] Beta-carotene is found in miniscule amounts in human arteries, however, it is a strong Raman scatterer and contributes to the artery spectrum by presenting a peak at 1130 cm^{-1} resulting from C-C and C=C stretching.[27,32] Amide III vibrations are evidenced by peaks at 1267 and 1303 cm^{-1}, while amide I vibrations are detected at 1656 cm^{-1}.[27,34,35] A dominant band appears at 1442 cm^{-1}; this peak is the result of CH_2 bending from cholesterol and its esters.[27,35] A peak located at 1749 cm^{-1} results from the C=O found in palmitic triglyceride.[36]

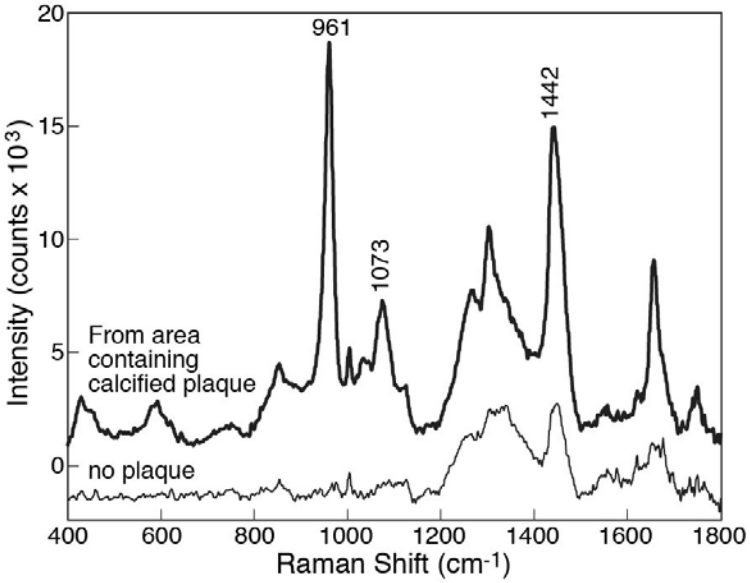

Figure 6. Representative micro-Raman spectra from human femoral artery. Major peaks are noted: 961cm^{-1}, phosphate from calcium hydroxyapatite; 1073cm^{-1}, carbonate from carbonate apatite; 1442cm^{-1}, cholesterol and cholesterol esters.

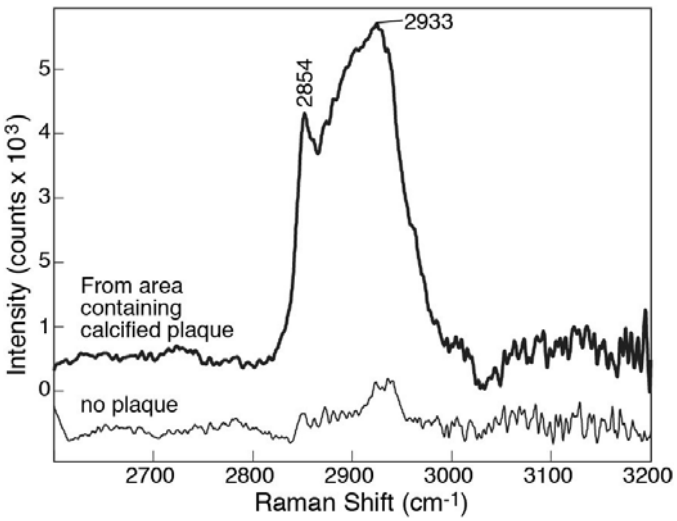

Figure 7. Representative micro-Raman spectra from human femoral artery in the spectral region 2800 to 3000cm^{-1}; peaks are associated with cholesterol and its esters.

Table 1. Tentative assignment and Raman peak positions observed with 785 nm excitation.

Frequency (cm^{-1})	**Assignment**
961	Phosphate symmetric stretching due to calcium hydroxyapatite[27,35]
1004	Phenylalanine aromatic ring[34]
1037	Phenylalanine aromatic ring
1073	Carbonate symmetric stretching due to carbonate apatite[27,35]
1130	C-C, C=C stretch mode from β-carotene accumulation[27,35]
1267	Amide III vibration[27]
1303	Amide III vibration, δ(CH)[34]
1442	CH_2 bending from cholesterol and cholesterol esters[27,35]
1656	Amide I vibration[35]
1749	C=O from palmitic triglyceride[36]

Chemical mapping based on prominent Raman peaks was also used to evaluate human femoral arteries. A 10x10 matrix of points was selected for Raman sampling for a total of 100 spectra from each area. Typical results are shown in Figs. 8, 9, and 10. Areas containing calcified plaques were identified by mapping the intensity of peaks 961 and 1073cm^{-1}. Areas containing high amounts of cholesterol were identified by mapping the intensity of the peak at 1442cm^{-1}. Figure 8 shows both a white light image and a Raman chemical map of an area of femoral artery. This map was generated using HoloMap software (Galactic) by mapping the intensity of the peak located at 961cm^{-1}. The areas of high intensity represent locations of high concentrations of phosphate from calcium hydroxyapatite within the vessel wall.

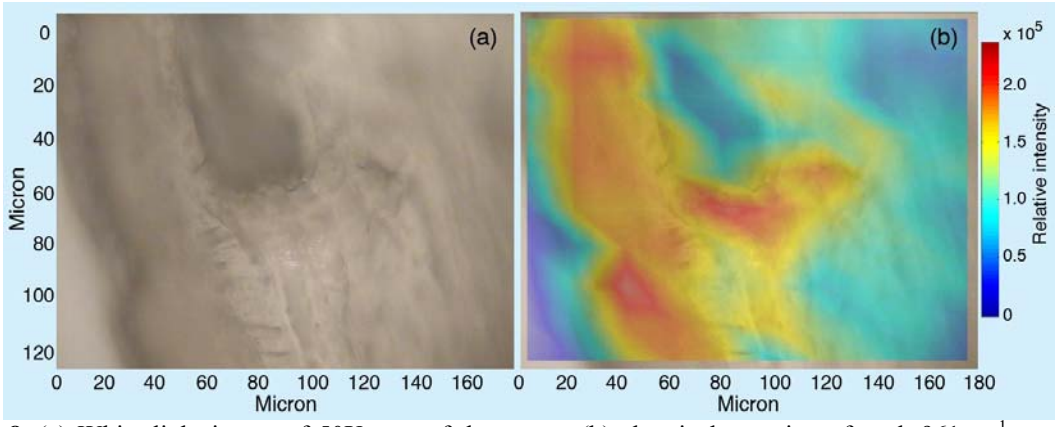

Figure 8. (a) White light image of 50X area of the artery; (b) chemical mapping of peak 961cm^{-1} overlay on white light image. Red areas indicate high peak intensity while blue areas are low intensity.

Similarly, Fig. 9 maps the intensity of the peak at 1073 cm^{-1}, which is indicative of carbonate present in carbonate apatite. Both calcium hydroxyapatite and carbonate apatite are known constituents of calcified atherosclerotic plaques.

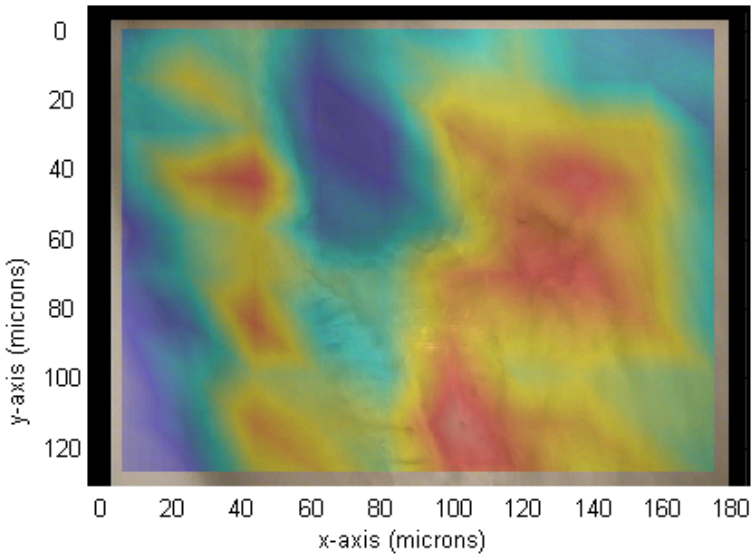

Figure 9. Chemical mapping of Raman peak 1073 cm^{-1} overlay on white light image. This peak represents the presence of carbonate in carbonate apatite in calcified plaques. Red areas indicate high peak intensity while blue areas are low intensity.

Figure 10 shows a chemical map based on the intensity of the Raman peak located at 1442cm^{-1}. This peak is associated with cholesterol and its esters. Cholesterol accumulates early in the atherosclerotic process. However, these cholesterol deposits are part of a calcified plaque. Figures 8, 9, and 10 are maps of the same area created using different Raman shifts. Examination

of the maps reveals that calcium hydroxyapatite, carbonate apatite, and cholesterol all co-localize within this site to form a large area of atherosclerotic plaque.

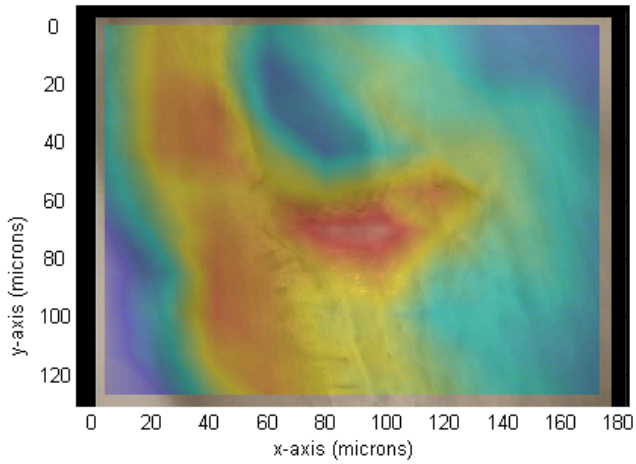

Figure 10. Chemical mapping of the Raman peak at 1442 cm^{-1} overlay on white light image. This peak represents the presence of cholesterol accumulations and may be sites of early plaque formations. Red areas indicate high peak intensity while blue areas are low intensity.

SERS technology can be applied to the study of atherosclerotic arteries through the use of immunohistochemistry techniques. Ten micron sections of human femoral artery mounted on aluminum slides were fixed and permeated by exposure to ice-cold methanol for 5 minutes. After rinsing three times with phosphate-buffered saline (PBS), arteries were blocked using 5% BSA in PBS for 1 hour. Sections were again rinsed three times with PBS before treatment with an antibody- DSNB-AuNP reporter as described above. Arteries were exposed to either anti-vWF-DSNB-AuNP or anti-Ki67-DSNB-AuNP reporters for 1 hour at room temperature. Slides were then rinsed three times in PBS and allowed to air dry before examination by Raman spectroscopy.

To understand the distribution of these proteins in arterial tissue, chemical mapping of areas of the artery was performed using antibody-labeled SERS reporters. A 10x10 matrix of points was selected for Raman sampling for a total of 100 spectra from each area. A typical spectrum of anti-vWF-DSNB-AuNP reporter is shown in Fig. 11. Prominent peaks indicate the presence of a DSNB SERS reporter. These peaks include 851 cm^{-1} (nitro scissoring vibration), 1076 cm^{-1} (succinimidyl N-C-O stretch overlapping with aromatic ring modes), 1333 cm^{-1} (symmetric nitro stretch), and 1558 cm^{-1} (aromatic ring mode {13a}). The primary band located at 1333 cm^{-1} was used for chemical mapping. Areas of high intensity (in red) represent areas where high concentrations of the target antigen have been recognized by the antibody-DSNB-AuNP complex. The representative chemical map results are shown in Fig. 12.

Anti-Ki67-DSNB-AuNP reporters revealed that the distribution of the Ki67 antigen is aggregated in discrete areas. Ki67 is a proliferation marker and is expected to be found in tissues exhibiting rapid growth. This protein is found in areas where there is a proliferation of

macrophages, which is a key step in the progression and destabilization of atherosclerotic plaques.[37] Anti-vWF-DSNB-AuNP reporters also found vWF to be allocated to concentrated areas of the artery. vWF is a glycoprotein that promotes the binding of platelets to sites of injury at vessel walls, an initial step in the formation of some types of atherosclerotic plaques.[38] Both Ki67 and vWF are markers for early stage atherosclerosis. Thus these SERS-based reporters can identify areas that will be vulnerable to plaque formation at later stages of development.

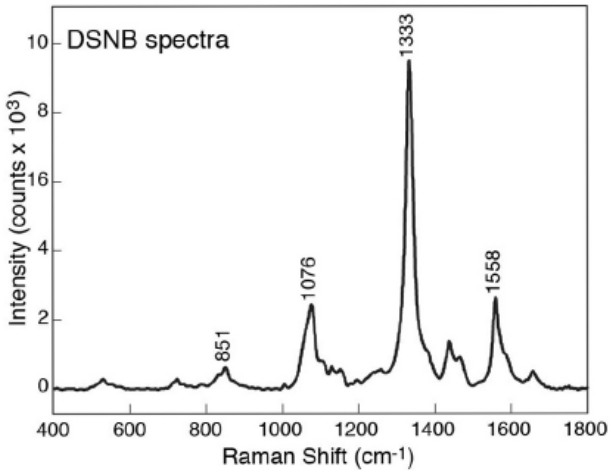

Figure 11. Representative anti-vWF-DSNB-AuNP reporter spectrum. Prominent DSNB peaks are labeled for clarity: 851 cm^{-1} (nitro scissoring vibration); 1076 cm^{-1} (succinimidyl N-C-O stretch overlapping with aromatic ring modes); 1333 cm^{-1} (symmetric nitro stretch); and 1558 cm^{-1} (aromatic ring mode (8a)). All SERS spectra were collected with the micro-Raman RXN system (Kaiser Optical Systems, Inc., Arbor, MI) using 10 mW of laser power and 60 s of integration time.

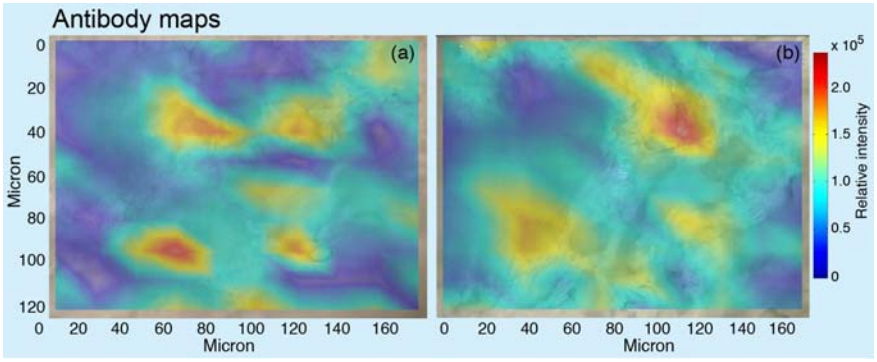

Figure 12. SERS detection of labeled antigens in human femoral arteries: (a) Distribution of anti-Ki67-DSNB-AuNP reporter in femoral artery tissue. (b) Distribution of anti-vWF-DSNB-AuNP reporter. Red indicates areas of high intensity while blue indicates areas of low intensity.

(iii) Micro-Raman and micro-SERS analysis of prostate cancer cell lines

With normal micro-Raman and micro-SERS analysis we investigated three cancer cell lines, DU145, PC3, and LNCaP, obtained from Dr. Michelle Herdman of University of Charleston School of Pharmacy, Charleston, WV. The DU145 cells, originally derived from prostate carcinoma and exhibiting an epithelial phenotype, are known to be insensitive to hormone treatment and do not produce PSA. PC3 cells were derived from a grade IV prostatic adenocarcinoma and also exhibit an epithelial morphology. These cells are androgen sensitive and are known to produce PSA in moderate amounts. LNCaP are the most differentiated of the three cell lines. They are derived from prostate carcinoma and have an epithelial morphology. These cells are also androgen sensitive and produce large amounts of PSA and prostatic acid phosphatase.

The average normal micro-Raman spectra of each cell line are shown in Figure 13. Each spectrum was collected at 20mW power for 240s. There are some noticeable differences between the spectra of these cell lines. The most notable of these is the presence of a peak at 936 cm^{-1} in the spectrum of the LNCaP cells. This peak is associated with the protein collagen and as previously noted in work from this laboratory is found in differentiated cells. This peak is found to be absent in the undifferentiated phenotypes associated with cancer cell lines such as cervical squamous cell carcinoma.[39] This is consistent with the characterization of these cell lines, where LNCaP is known to be a more differentiated, slower-growing cell line while DU145 and PC3 cells are dedifferentiated and faster-growing. Other notable peaks are listed in Table 2.

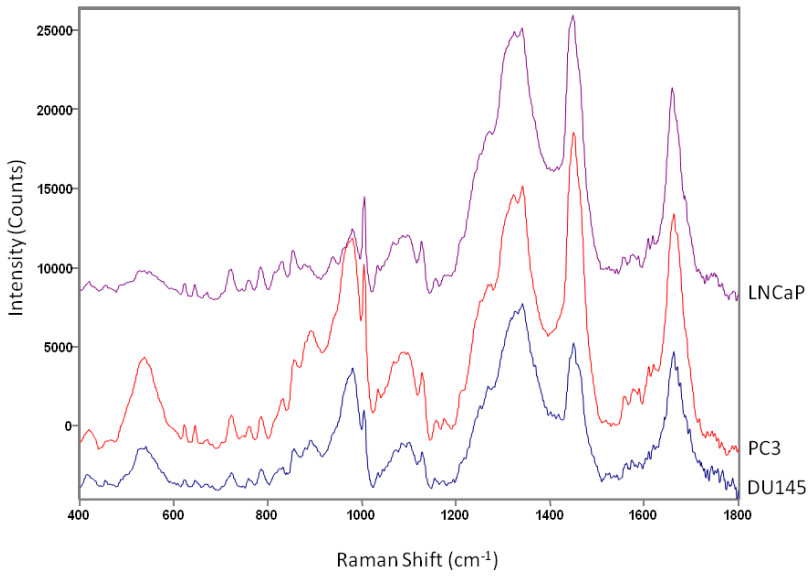

Figure 13. Average spectra of three prostate cancer cell lines collected at 20mW for 240s. Each spectrum is the average of ten individual spectra.

Table 2. Normal Raman peak positions and assignments of prostate cancer cells in three cell lines

Raman shift	Cell Line			
cm^{-1}	DU145	PC3	LNCaP	Assignments
537, 540	+	+	+	δ(C-O-C) glycosidic ring[40]
622	+	+	+	C-C twisting, Phe[41]
644	+	+	+	C-C twisting, Tyr[41]
670		+	+	G, T[41]
721, 722	+	+	+	Choline[41]
758, 759	+	+	+	Trp ring breathing[41]
783, 784	+	+	+	U, C, T ring breathing[41]
830		+	+	O-P-O asymmetric stretch, Tyr ring breathing[41]
853, 854	+	+	+	Tyr ring breathin[41]
878			+	acyl C2-C1 stretch (lipid)[11]
936			+	C-C symmetrical stretch backbone, α-helix[41]
977, 978	+	+	+	head C-C stretch (lipid) [41]
1003	+	+	+	Phe symmetrical ring breathing[41]
1032	+	+	+	C-H Phe[41]
1065, 1066		+	+	C-N stretch, lipid chain C-C stretching[41]
1088	+			DNA($O\text{-}P\text{-}O^-$)[40]
1095, 1099	+	+	+	PO_2^- backbone, C-N stretch, lipid chain C-C stretching[41]
1125, 1126	+	+	+	C-N stretch, lipid chain C-C stretching[41]
1153, 1155	+	+	+	C-C, C-N stretching[41]
1173. 1174		+	+	C-H Tyr, Phe[41]
1249	+			Amide III β-sheet[41]
1266, 1270	+		+	Amide III α-helix, lipid =CH deformation[41]
1320, 1323		+	+	C, CH deformation[41]
1338	+	+	+	A, G, CH deformation[41]
1447	+	+	+	protein C-H deformation, lipid C-H deformation[41]
1658, 1659	+	+	+	Amide I α-helix, lipid C=C stretching[41]
1667			+	Amide I[41]
1685			+	Amide I β-sheet[41]
2850, 2870	+			lipid C-H stretching vibrations[42,43]
2880, 2881	+	+	+	C-H stretching mode[41]
2887	+			CH_2 asymmetrical stretch[41]
2896	+	+	+	C-H stretching, cholesterol ester[44]
2932	+	+	+	CH_3 symmetrical stretching[41]
2939	+			C-H stretching vibrations[40]
2961, 2962	+	+	+	CH_3 symmetrical stretching[41]

Cells were also incubated with gold nanoparticles (AuNPs) prior to study by SERS microscopy. AuNPs were prepared as previously described. Then, one ml of AuNPs was centrifuged at 10,000g for 7 minutes. The supernatant was discarded and the AuNPs were resuspended in 1 ml sterile PBS. These sterile AuNPs were added to each cell line by supplementing cell culture medium at a ratio of 1:15. The cells were incubated with AuNPs for 24 hours before harvesting for Raman spectroscopic interrogation. The resulting SERS spectra are shown in Fig. 14.

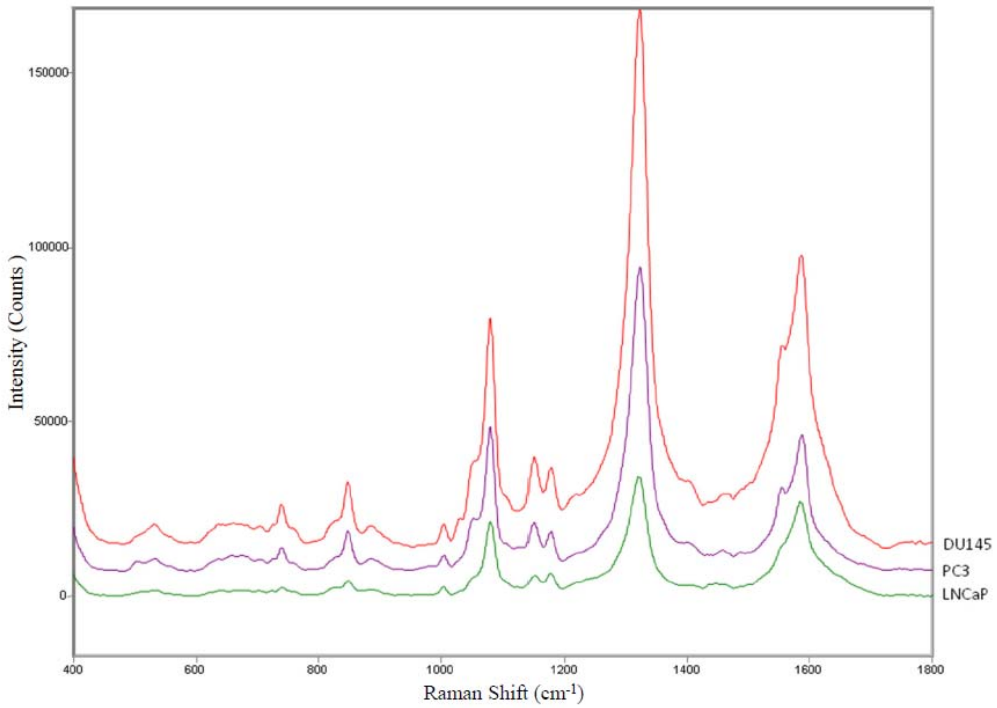

Figure 14. Averaged SERS spectra of prostate cancer cell lines incubated with AuNPs. Spectra were collected at 20 mW for 30 s

Prominent SERS peaks in the spectra of prostate cancer cell lines and their tentative assignments are listed in Table 3. It has been previously demonstrated that AuNP taken up by endocytosis are mostly trapped inside lysosomes or endosomes.[45] The peak assignments listed in Table 2 support this theory. A large number of peaks are associated with nucleic acids (A, C, T, G) and some with phosphate groups. Because of lysosomal RNA degradation, large amounts of nucleosides and phosphates are known to reside within lysosomes.[46] Thus it is reasonable to assume the accumulation of AuNPs in the lysosomes, which are known accumulation points for nanoparticles.[47] Some AuNP are also associated with mitochondria, another known accumulation point for nanoparticles.[48]

Table 3. SERS Raman peaks in the spectra of prostate cells and their tentative assignments

Raman Shift (cm^{-1})	Assignment
847	Ring breathing, C-H stretching vibration
887	Mitochondria[48]
1004	Phe
1030	Phe, mitochondria[48]
1080	C-C, C-O, PO_2, C-N, O-P-O; vibrational modes of nucleic acids, proteins, and carbohydrates
1150	C-C, C-N stretching
1177	T, C, G, C-H, Tyr, Phe[34]
1323	C-H deformation, G, C, protonated A residues[34]
1585	G, CO_2 stretching [34]

We also measured the micro-Raman spectra of a pellet of human prostate tumor cells DU145 to compare our results with the published micro-Raman data of Mathews et al. (2010).[49] For this study, the human carcinoma epithelial cell line DU145 was cultured in Eagle's Minimum Essential Medium supplemented by 10% Fetal Bovine Serum. No antibiotics were added to the cell culture medium. The cells were incubated in T-75 flask equipped with a 0.2 µm mesh lid. The cell culture medium was changed two to three times a week. The DU145 cells were incubated in a humidified atmosphere at 37 °C with 5% CO_2 and 95% relative humidity.

In preparation for micro-Raman spectroscopy 1.2×10^7 cells were centrifuged at 125 g and 4° C. Prior to centrifugation circular aluminum slides were prepared so as to fit into the wells of a 24-well multi-plate cell culture dish. Figure 15 shows the baseline corrected micro-Raman spectra of the individual cells in the pellet of DU145 tumor cells measured with 50x objective as a function of depth from the surface of the pellet. The origins of the identifiable features are marked on the spectra.

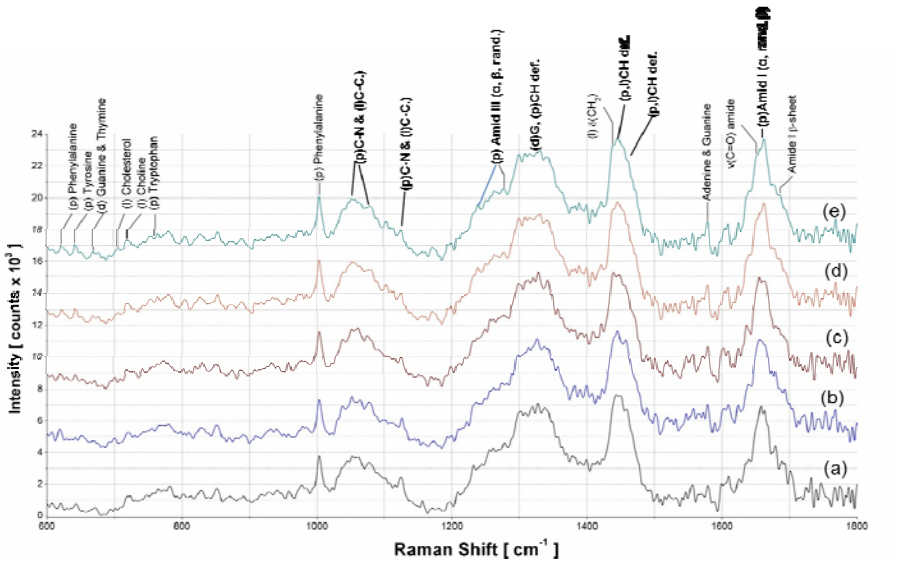

Figure 15. Micro-Raman spectra of DU145 cells as a function of depth (a) cells on the surface, and at the depth of (b) 1 µm, (c) 2 µm, (c) 3 µm, (d) 4 µm, and (e) 5 µm. Laser 785 nm, 60 s, 5 accumulations. Abbreviations: (p) protein; (l) lipid; and (d) DNA/RNA.

The Raman spectra of DU 145 in Fig. 15 show close resemblance to each other. These spectra are also similar to those reported by Mathews et al. (2010).[41]

(iv) Micro-SERS analysis of exfoliated cells from urine sample

Different types of epithelial cells can be observed in urine. Some of these are readily identifiable; however, it is difficult to distinguish small transitional epithelial cells from white blood cells or renal tubular epithelial cells. We began our preliminary examination of exfoliated cells from urine with micro-surface-enhanced Raman scattering (SERS) spectroscopy. First-void urine (FVU) samples were provided by a healthy volunteer. The samples were allowed one hour to equilibrate to room temperature. Subsequently, 120 mL of the FVU samples were centrifuged in series at 4 °C and 350 ×g. In order to isolate the exfoliated urine cells from the urine, the samples were washed in three centrifugal steps with Dulbecco's Phosphate Buffered Saline (DPBS) at 4 °C and 350 ×g. The DPBS pH was 7.4 at 23 °C. Before the last centrifugation, the DPBS solution with the exfoliated urine cells was transferred into a 12-well culture multiwell plate. Prior to the transfer, round aluminum substrates were prepared with 38-45 μm cavities and placed into the wells of the multiwell culture plate. During the final centrifugation the exfoliated cells, gold nanoparticles (AuNPs) were added and the cells mounted onto the aluminum slides. The slides were removed from the plate and dried under a weak nitrogen air stream before acquiring micro-Raman spectra.

The presence of AuNP on and inside exfoliated cells allowed measurement of the micro-Raman spectra of individual cells with 1 s integration time because of surface-enhanced effect caused by the Au nanoparticle. Figure 16 shows the micrographs of individual cells in the insert, and their SERS spectra of respective cells. The set A of the cells consisting of cells #2, #3, #6, #8 and #9 have similar spectral features and are round in shape. There is, however, a change in the relative intensities of the peaks (Table 4). The second set B of the cells consisting of cells #1, #7 and #10 are round in shape but show different SERS spectra (Fig. 17). The cell #4 has a distinct Raman spectrum and is elongated in shape (Fig. 18). The intensity of Amid-I bands in the 1600-1650 cm^{-1} region are lower in the set A cells (Table 4) than those in the spectra of the cells in set B, and cell #4 (see Table 5). Tentative assignments of various Raman peaks are listed in Tables 4 and 5 based on previous assignments made by Movasaghi et al.[50] The difference in the intensities of the Amide I bands indicate that the proteins to lipids content of the cells in set A is higher than those in set B (e.g., Takai et al.[51]). Evidently, based on the chemical composition of the cells, it is possible to use the SERS spectra of the exfoliated cells to identify various types of cells from the urine samples of patients.

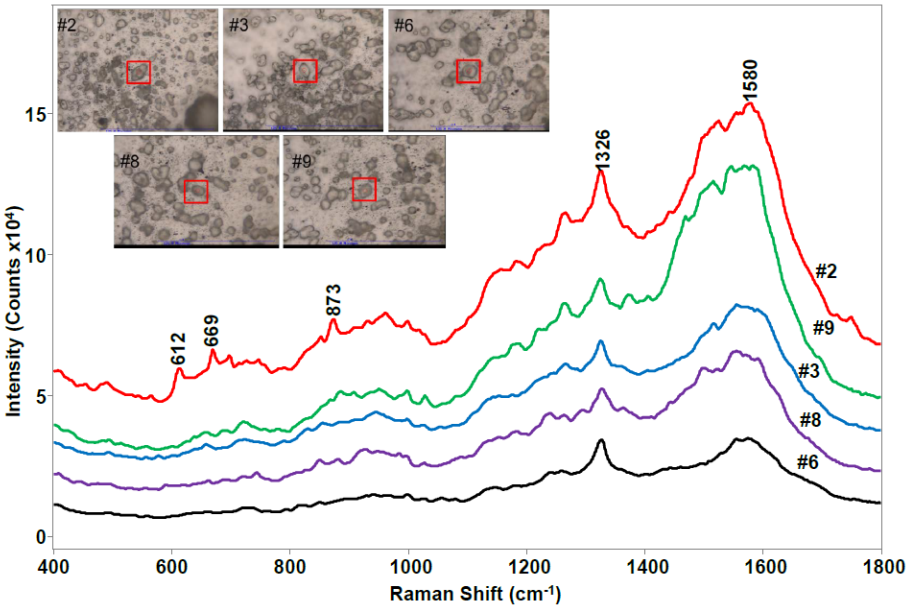

Figure 16. Micro-SERS spectra of exfoliated cells #2, #3, #6, #8 and #9 of set A from the urine of a healthy volunteer with 50 x objective. The centers of the red squares mark the cell positions. The blue scale at the bottom of each figure is 150 µm long. Laser 785 nm, 10 mW, integration time 1 s, 10 accumulations.

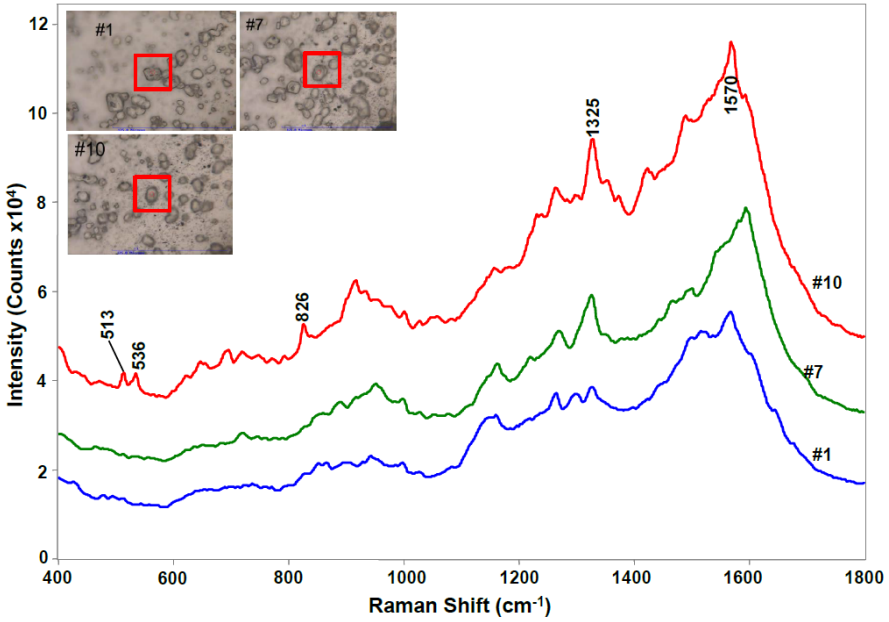

Figure 17. Micro-SERS spectra of exfoliated cells #1, #7, and #10 of set B from the urine of a healthy volunteer with 50 x objective. The red square marks the cell position. Experimental conditions are the same as in Fig. 16

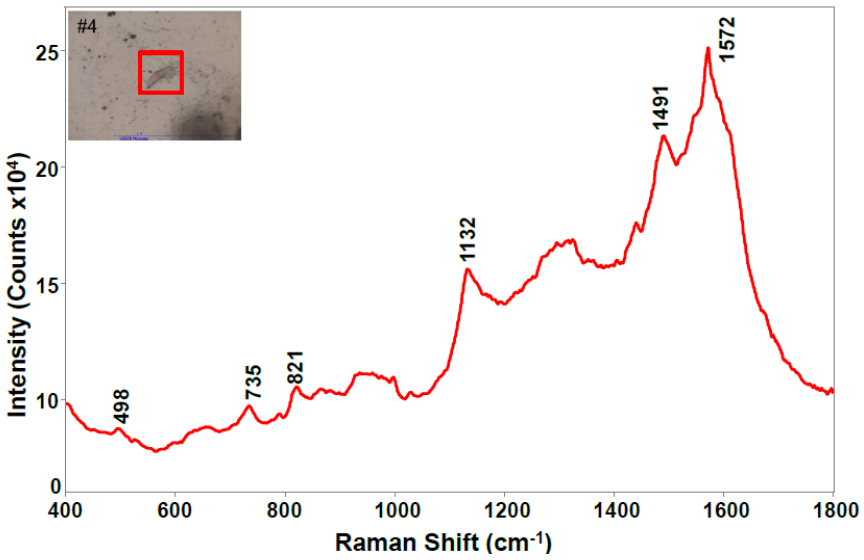

Figure 18. Micro-SERS spectra of exfoliated cell no. #4 from the urine of a healthy volunteer with 50 x objective. The red square marks the cell position. Experimental conditions are the same as in Fig. 16.

Table 4. Raman peak positions and their relative intensity in the spectra of exfoliated cells in set A from urine samples
(*Rel. I = Relative percentage peak height with respect to the intensity of the strongest Raman peak)

Cell #2		**Cell #3**		**Cell #6**		**Cell #8**		**Cell #9**		**Tentative Assignments** (after Ref.[50])
Δv cm^{-1}	**Rel. I**	**Δv cm^{-1}**	**Rel. I***	**Δv cm^{-1}**	**Rel. I**	**Δv cm^{-1}**	**Rel. I**	**Δv cm^{-1}**	**Rel. I**	
		408	3	408	3	410	5	405	1	
413	7	418	<1	418	<1	415	2	420	1	
424	7	433	1			424	1	426	2	
431	7			433	1			433	2	
454	4	463	<1			446	5	441	<1	Ring torsion of phenyl
465	4			463	1	464	2			
				482	5	475	5			
490	20	495	16	497	6	495	7	494	10	Glycogen
513	12	513	4	513	4	515	1	514	9	
				524	2	529	2			S-S stretch
		535	5	535	6	540	<1			Cholesterol ester
543	6	557	3	557	3	558	2	557	7	
564	7									
		579	<1			571	1			Phosphatidylinositol
				597	1	590	6	599	4	Nucleotide confirmation
		600	7							Nucleotide confirmation
				607	1					Cholesterol
612	28									Cholesterol ester
						619	4			C-C twist proteins
		638	14	636	9	637	3	638	9	v(C-S) gauche (amino acid methionine)
						653	3			
669	37	658	20	659	10	662	4	657	11	C-S stretching mode of cytosine
		683	<1	686	7	686	8	686	10	
697	9			694	8	690	9			v(C-S) trans (amino acid methionine)
725	17	722	20	723	16	721	12	721	14	DNA

Table 4 (continued)										
Cell #2		**Cell #3**		**Cell #6**		**Cell #8**		**Cell #9**		**Tentative Assignments** (after Ref.[42])
Δv cm^{-1}	**Rel. I**	**Δv cm^{-1}**	**Rel. I**	**Δv cm^{-1}**	**Rel. I**	**Δv cm^{-1}**	**Rel. I**	**Δv cm^{-1}**	**Rel. I**	
746	15			758	<1	743	16			Tryptophan, ethanolamine group, phosphatidylethanolamine,
760	2									Tryptophan, δ ring (proteins)
								778	3	Phosphatidylinositol
		789	<1							Phosphatidylserine
				793	2					Backbone geometry & phosphate ion
				817	14					C-C stretch (Collagen assignment)
		829	25			826	14			O-P-O stretch
852	7	855	33	850	18	850	28	868	22	polysaccharide structure
						881	28			Tryptophan, δ (ring)
873	42	884	32					885	28	Protein, including collagen I
908	31	910	34	894	3			908	26	Sugar
				929	28	926	41			C-C stretch amino acids (protein)
				940	29	946	5			Skeletal mode polysaccharides
		946	45					950	26	Skeletal mode polysaccharide
				961	26					Symmetric stretch PO_4^{3-}
						984	23			C-C stretch β-sheet (protein), =CH bending (lipids)
998	12	998	6	998	26	996	19	997	21	C-O ribose, C-C
1018	11									
1026	8	1024	5	1027	13	1026	7	1028	14	Glycogen
		1052	5							Glycogen
1050	6			1056	12			1059	4	Lipid
1081	15	1080	4	1079	4	1089	7	1080	7	Sugars
1145	59	1143	46	1144	24	1135	28	1144	30	
1156	60	1153	46			1151	31			C-C (& C-N) stretch of protein, =C-C= carotenoid
		1175	43			1177	35	1176	34	Cytosine, guanine
1181	62			1182	23	1183	35			Cytosine, guanine, adenine

Table 4 (continued)										
Cell #2		**Cell #3**		**Cell #6**		**Cell #8**		**Cell #9**		**Tentative Assignments** (after Ref.[50])
Δv cm^{-1}	**Rel. I**	**Δv cm^{-1}**	**Rel. I**	**Δv cm^{-1}**	**Rel. I**	**Δv cm^{-1}**	**Rel. I**	**Δv cm^{-1}**	**Rel. I**	
1218	62			1206	22			1219	37	Amide III (protein)
1229	63	1229	61							Amide III (protein)
		1240	63	1240	43	1239	53			Amide III (protein)
		1244	63							Amide III (protein)
1261	83	1265	73	1258	41	1262	7	1263	47	Amide III (protein)
						1293	9			Amide III (protein)
1325	100	1325	95	1326	100	1327	72	1324	48	CH_3CH_2 wagging mode in collagen & purine base of DNA
						1362	7	1372	9	Guanine
		1395	5							CH rocking
1405	6	1403	6	1400	2	1398	4	1405	3	N-H plan deformation
1421	6									CH_2 scissoring vibration (lipids)
1428	4			1432	7					CH_2 bending mode of proteins and lipids
1441	4			1443	9	1442	5			Cholesterol
		1456	7							Deoxyribose
				1461	7					CH_2/CH_3 deformation (lipids & collagen)
		1470	11					1469	57	C=N stretching
1478	32									Amide II*
				1495	3	1498	71			Amide II
1502	67							1503	76	Amide II
				1510	15					Adenine (ring breathing mode in DNA bases)
		1515	19					1515	81	Amide II
1521	76					1521	68			Amide II, Carotenoid -C=C-
1525	77			1529	2	1524	68			Amide II, Carotenoid -C=C- in plan vibration
1555	85	1556	100	1555	64	1555	100	1546	94	Tryptophan, ν(CN) & δ(NH) amid II(protein)
								1567	96	COO^-
		1573	98	1575	67	1572	96	1571	97	Guanine, adenine, transient receptor potential (TRP) protein

Table 4 (continued)										
Cell #2		**Cell #3**		**Cell #6**		**Cell #8**		**Cell #9**		**Tentative Assignments** (after Ref.[42])
Δv cm^{-1}	**Rel. I**	**Δv cm^{-1}**	**Rel. I**	**Δv cm^{-1}**	**Rel. I**	**Δv cm^{-1}**	**Rel. I**	**Δv cm^{-1}**	**Rel. I**	
1580	97	1581	97					1583	100	Amide II**
1590	5	1590	98			1591	94			C=N & C= C stretching in quinoid ring
				1664	2					Amide I
						1677	3			Bound and free NADH
1684	3	1682	5	1684	2			1684	4	Amide I (disordered structure, non-hydrogen bonded)
**Amide II largely due to a coupling of CN stretch and in-plan bending of NH group.										

Table 5. Raman peak positions and their relative intensity in the spectra of the cells in set B and cell#4 from urine samples
(*Rel. I = Relative percentage peak height with respect to the intensity of the strongest Raman peak)

Cell #1		**Cell #7**		**Cell #10**		**Cell #4**		**Tentative Assignment** (after Ref.[50])
Δν (cm^{-1})	**Rel. I**	**Δν (cm^{-1})**	**Rel. I**	**Δν (cm^{-1})**	**Rel. I**	**Δν (cm^{-1})**	**Rel. I**	
		405	4	407	4	407	1	
410	3	412	3					
		422	4					
429	15			434	3	432	0	
451	2	452	2	445	3	454	3	Ring torsion of phenyl
		464	6	471	4	464	1	
479	13	479	9	478	1	473	5	
492	9			485	3	488	7	Glycogen
501	12	496	7	497	4	498	9	
513	13	513	6	513	16	509	7	
525	6	527	2	526	8	524	5	S-S stretching in protein
535	4	536	5	534	17	533	5	Cholesterol ester
544	7			544	5	544	2	Glucose-saccharide band
556	5	556	1	554	3	553	2	
566	4	562	3	565	2			
573	3			577	1	574	1	Tryptophan/cytosine, guanine
600	7			599	3	598	4	Nucleotide confirmation
609	7	604	3	609	5	608	1	Cholesterol
						617	4	Cholesterol ester
625	19	621	8	621	13	625	7	C-C twisting mode of phenylalanine (protein)
638	16	635	8	635	9	634	6	ν(C-S) gauche (amino acids methionine)
647	10	647	8	645	15	644	8	C-C twisting mode of tyrosine
654	3			658	15	655	7	
662	23	663	8			662	5	C-S stretching mode of cytosine
						669	4	Guanine
				673	11	675	1	Ring breathing mode of DNA bases
689	21	683	8	687	19	687	3	
696	1	697	6	697	13			
702	10			712	10	702	2	Cholesterol, cholesterol ester

Table 5 (continued)

Cell #1		Cell #7		Cell #10		Cell #4		**Tentative Assignment** (after Ref.[42])
Δν (cm^{-1})	**Rel. I**	**Δν (cm^{-1})**	**Rel. I**	**Δν (cm^{-1})**	**Rel. I**	**Δν (cm^{-1})**	**Rel. I**	
711	3					708	2	
		718	17	719	8	719	7	C-N (membrane phospholipid head);
723	8					728	7	DNA
737	11			731	7	735	10	C-S stretching mode
745	4	744	8	746	10	742	7	
757	5	759	3	756	3	752	2	Sym. breathing tryptophan
762	1					762	<1	Tryptophan, δ ring (proteins)
771	5	773	3	770	5	776	<1	
796	6			792	3	789	3	
		804	9	810	1			Phosphodiester (Z-marker)
816	2							C-C stretching
828	21	827	15	826	19	821	17	O-P-O stretch; tyrosine buried
				839	11	840	7	Exposed tyrosine
		844	10					
851	34	859	30	859	13	857	10	Polysaccharide structure
866	26			870	7	868	8	Ribose vibration, one of distinct RNA modes
878	4							C-OC ring carbohydrate
885	16	888	39	882	16	882	11	C-O-C skeletal mode
895	3					899	7	Backbone, C-C skeletal
904	23			900	27			
		913	29	915	40	915	7	Ribose vibration of RNA
929	16	929	4			927	8	C-C stretch amino acids (protein)
				933	34	937	14	Proline, hyroxyproline, ν(C-C) skeletal of collagen backbone
941	20	950	58	949	15	947	3	Skeletal mode polysaccharide
953	19			957	12	961	18	$\nu_s(CH_3)$ α-helix
968	2			969	10			Lipids
				977	12	976	7	Ribose vibration of RNA
985	5	983	12			985	11	C-C stretch β-sheet (protein), =CH bending (lipids)
994	12	998	27			997	15	C-O ribose, C-C

Table 5 (continued)

Cell #1		**Cell #7**		**Cell #10**		**Cell #4**		**Tentative Assignment** (after Ref.[42])
Δν (cm^{-1})	**Rel. I**	**Δν (cm^{-1})**	**Rel. I**	**Δν (cm^{-1})**	**Rel. I**	**Δν (cm^{-1})**	**Rel. I**	
		1022	15	1020	3	1029	3	Glycogen
				1027	5			O-CH_3 stretch methoxy group
				1043	3			Carbohydrate (collagen)
				1047	3			Glycogen
		1053	7	1057	3			Lipids
				1060	2			C-C stretching (lipids & carbohydrates)
1082	9	1074	4	1080	1	1084	4	Sugars
		1107	5			1100	10	Carbohydrate
1113	15			1114	2	1114	26	
				1127	5			Sugars
				1135	6	1132	65	Fatty acids
1144	71	1144	33	1144	10	1149	47	Carbohydrate
1158	33			1155	18			C-C, C-N stretch in protein; =C-C= carotenoid;
		1160	17	1162	6	1163	34	Tyrosine (collagen type I)
		1174	23	1171	5	1179	37	Tyrosine (collagen type I)
				1179	13			Cytosine & guanine
				1182	3			Cytosine, guanine and adenine
		1201	18	1194	6	1194	19	Nucleic acids & phosphates; aromatic C-O & C-N
1214	65	1218	34	1218	25	1218	36	C-N stretch
1235	10	1239	29	1238	31	1240	17	Amide III
						1248	17	Amide III
1264	82	1267	56	1263	50	1267	35	Fatty acids
				1283	28	1282	27	Collagen type I
1297	41			1298	30	1296	37	Fatty acids
		1305	41					CH_2 deformation (lipids), adenine, cytosine
		1314	2			1313	26	CH_3CH_2 twisting mode collagen
1324	70			1325	69	1327	31	CH_3CH_2 wagging mode in collagen & purine base of DNA
		1351	20	1353	30	1352	1	Guanine
		1378	7	1371	13	1384	2	Polysaccharide

Table 5 (continued)

Cell #1		Cell #7		Cell #10		Cell #4		**Tentative Assignment** (after Ref.[50])
Δν (cm^{-1})	**Rel. I**	**Δν (cm^{-1})**	**Rel. I**	**Δν (cm^{-1})**	**Rel. I**	**Δν (cm^{-1})**	**Rel. I**	
1001	13			1000	11			Phenylalanine
				1421	21	1426	1	Breathing mode of adenine & Guanine
				1429	9			Deoxyribose
				1444	19	1441	14	Cholesterol
		1462	12	1457	20	1460	14	Sucrose
		1470	5	1473	29	1471	14	C=N stretching
1474	46	1477	6			1478	28	Amide II
				1488	51	1490	46	Collagen
1493	56	1491	14					C-N Stretch couple with C-H stretch
				1506	50	1504	42	N=H bending, Cytosine
1514	93			1524	57	1520	30	Carotenoid
						1536	45	Amide carbonyl group & aromatic hydrogen
1547	85	-	-	1542	70	1546	23	Bound & free NADH
1568	100	1557	40	1557	24	1556	61	Amide II
		1572	40	1570	100	1571	100	Ring stretch guanine & adenine (protein)
1584	20	1580	45			1583	61	C-C stretch
		1594	100	1592	54	1594	54	C=N & C=C stretching in quinoid ring
1600	81	1609	66	1607	53	1610	70	Amide I band of proteins due to C=O stretching
		1624	25	1626	28			Tryptophan &/or β-sheet
		1633	24			1631	24	Amide I
1648	12							Random coil

KEY RESEARCH ACCOMPLISHMENTS

- Established the Raman Biomedical Research Program at the University of Hawaii in collaboration with Tripler Army Medical Center (TAMC).
- Obtained approval from the University of Hawaii Committee on Human Studies (CHS) on October 20, 2010.
- Developed SERS-based immunoassay for detecting PSA using nitrocellulose as substrate.
- Prepared TAMC IRB application, submission completed on July 11, 2011.
- Obtained continuing approval from the University of Hawaii CHS on August 26, 2011.
- Obtained continuing approval from the University of Hawaii CHS on July 12, 2012.
- TAMC IRB application approved by the Scientific Review Committee on July 19, 2012.
- Micro-Raman imaging of tissue samples.
- Micro-Raman and micro-SERS examination of prostate cancer cell lines.
- Micro-SERS investigation of exfoliated cells from urine samples.
- The CRADA between TAMC and UH was submitted to JAG for approval. It was approved by JAG on September 21, 2012 and forwarded to Command for Approval.
- TAMC protocol approved by the Clinical Investigation Regulatory Office (CIRO) on October 14, 2012.

REPORTABLE OUTCOMES

- Manuscript entitled "Nitrocellulose-based SERS based immunosensor for detection of biological molecules" was published in the *Proceedings of Smart Biomedical and Physiological Sensor Technology VIII,* Eds. Brian M. Cullum and Eric S. McLamore, Proc. SPIE, **8025**, 802503/1-802503/11 (2011). (for reprint see Appendix IV)
- Manuscript entitled "*In vitro* quantitation of human femoral artery atherosclerosis using near-infrared Raman spectroscopy" was published in the *Proceedings of Smart Biomedical and Physiological Sensor Technology IX,* Eds. Brian M. Cullum and Eric S. McLamore, Proc. SPIE, **8367**, 836705/1-836705/10 (2012). (for reprint see Appendix V)

CONCLUSION

The nitrocellulose membrane has proven to be an effective medium for antigen capture. Nitrocellulose offers comparable results to those obtained using gold-coated glass substrates while offering a more cost-effective and time-saving method of immunoassay. While nitrocellulose is a Raman-active material, it does not interfere with immunoassay results because nitrocellulose Raman peaks are distinct from those of our DSNB reporter molecule. Micro-Raman imaging technology was found to be effective in chemical mapping of arteries in the tissues, indicating that it will be possible to detect differences in normal and diseased tissues. Both micro-Raman and micro-SERS analysis was able to characterize the biochemistry at the molecular level of three types of prostate cancer cell lines (DU145, PC3, and LNCaP); and micro-SERS analysis of exfoliated cells from a urine sample of a healthy volunteer showed the potential of the technique as the SERS spectra of individual cells can be measured, and various types of cells can be differentiated on the basis of their spectra.

REFERENCES

[1] Tu, A.T., *Raman Spectroscopy in Biology: Principles and Applications*, Wiley, New York, (1982).

[2] Parker, F. S., *Applications of Infrared, Raman, and Resonance Raman Spectroscopy in Biochemistry*, Plenum Press, New York (1983).

[3] Spiro, T. G. (1987) *Biological applications of Raman spectroscopy*, Wiley, New York (1987).

[4] Manfait, M., S. Charonov, I. Chourpa, and P. Valisa, Confocal Raman microscopic imaging of biological materials, Proc. SPIE, 2980, 210-216 (1997).

[5] Gremlich, H.-U. and B. Yan (eds.) *Infrared and Raman Spectroscopy of Biological Materials*, Marcel Dekker, New York (2001).

[6] Vo-Dinh, T., D. L. Stokes, G. D. Griffin, M. Volkan, U. J. Kim, and M. I. Simon, "Surface-enhanced Raman Scattering (SERS) method and instrumentation for genomics and biomedical analysis", J. Raman Spectrosc. 30, 785-793 (1999).

[7] Kneipp, K., H. Kneipp, I. Itzkan, R. Dasari, and M. Feld, "Surface-enhanced Raman scattering and biophysics", J. Phys. Condens. Matter, 14, R597-R624 (2002).

[8] Fenn, M. B., P. Xanthopoulos, G. Pyrgiotakis, S. R. Grobmyer, P. M. Pardalos, and L. L. Hench, "Raman spectroscopy for clinical oncology, Advances in Optical Technologies", 2011:20, (2011). Article ID 213783, doi:10.1155/2011/213783

[9] Kambhampati, P., C. M. Child, M. C. Foster, and A. Campion, "On the chemical mechanism of surface enhanced Raman scattering: Experiment and theory", J. Chem. Phys., 108, 5013-5026 (1998).

[10] Porter, M. D., R. J. Lipert, L. M. Siperko, G. Wang, and R. Narayanana, "SERS as a bioassay platform: fundamentals, design, and applications", Chem. Soc. Rev., 37, 1001-1011 (2008).

[11] Hering, K., D. Cialla, K. Ackermann, T. Dorfer, R. Moller, H. Schneidewind, R. Mattheis, W. Fritzsche, P. Rosch, and J. Popp, "SERS: a versatile tool in chemical and biochemical diagnostics", Anal. Bioanal. Chem., 390, 113-124 (2008).

[12] Chen, J. W., J. H. Jiang, X. Gao, J. L. Gong, Shen, and R. Q.,Yu, "Gold-aggregated, dye-embedded, polymer-protected nanoparticles (GDPNs): A new type of tags for detection with SERS", Colloid Surface, A 294, 80-85 (2007).

[13] Grubisha, D. S., R. J. Lipert, H. Y. Park, J. Driskell, and M. D. Porter, "Femtomolar detection of prostate-specific antigen: an immunoassay based on surface-enhanced Raman scattering and immunogold labels", Anal. Chem. 75, 5936-5943 (2003).

[14] Jemal, A., R. Siegel, E. Ward, T. Murray, J. Xu, and M. J. Thun, "Cancer statistics, 2007", CA Cancer J. Clin., 57, 43-66 (2007).

[15] www.cancer.gov/cancertopics/factsheet/Detection/early-prostate

[16] Yu, H., E. P. Diamandis, A. F Prestigiacomo, and T. A. Stamey, "Ultrasensitive assay of prostate-specific antigen used for early detection of prostate cancer relapse and estimation of tumor-doubling time after radical prostatectomy", Clin. Chem. 41, 430-434 (1995).

[17] Morcol T., and A. Subramanian, "A red-dot-blot protein assay technique in the low nanogram range", Anal. Biochem., 270, 75-82 (1999).

[18] Nezlin, R., "A quantitative approach to the determination of antigen in immune complexes", J. Immun. Methods, 237, 1-17 (2000).

[19] Noya, O. and B. A. de Noya, "The multiple antigen blot assay (MABA): a simple immunoenzymatic technique for simultaneous screening of multiple antigens", Immun. Letts., 63, 53-56 (1998).

[20] Nakamura, K., T. Tanaka, A. Kuwahara, and K. Takeo, "Microassay for proteins on nitrocellulose filter using protein dye-staining procedure", Anal. Biochem. 148, 311-319 (1985).

[21] Lin, C. C., Y. M. Yang, Y. F. Chen, T. S. Yang, and H. C. Chang, "A new protein A assay based on Raman reporter labeled immunogold nanoparticles", Biosens. Bioelectron., 24, (2008).

[22] Dykes, A. C., L. Kamemoto, A. K. Misra *et al.*, "Nitrocellulose-based SERS immunosensor for detection of biological molecules", Proc. SPIE, 8025, 802503 (2011).

[23] Saraiva, S. A. and J. F. de Oliveira, "Control of particle size in the preparation of colloidal gold," J. Dispersion Sci. Technol., 23, 93–123 (2002).

[24] Lazarides, A. A. and G. C. Schatz, "DNA-linked metal nanosphere materials: Structural basis for the optical properties", J. Phys. Chem., B 104, 2987-2993 (2000).

[25] Nash, A. F. and I. Melezinek, "The role of prostate specific antigen measurement in the detection and management of prostate cancer", Endocr. Relat. Cancer, 7, 37-51(2000).

[26] Vassilikos, E. J. K., H. Yu, J. Trachtenberg, R. K. Nam, S. A. Narod, I. L. Bromberg, and E. P. Diamandis, "Relapse and cure rates of prostate cancer patients after radical prostatectomy and 5 years of follow-up", Clin. Biochem. 33, 115- 123 (2000).

[27] Silveira, L., S. Sathaiah, R. A. Zangaro, *et al.*, "Correlation between near-infrared Raman spectroscopy and the histopathological analysis of atherosclerosis in human coronary arteries", Lasers Surg. Med., 30(4), 290-297 (2002).

[28] Lloyd-Jones, D., "Heart disease and stroke statistics-2009 Update: A report from the American Heart Association Statistics Committee and Stroke Statistics Subcommittee (vol. 119, p. e21, 2009) ", Circulation, 122(1), E11-E11 (2010).

[29] Cassar, A., D. Poldermans, C. S. Rihal *et al.*, "The management of combined coronary artery disease and peripheral vascular disease", Euro Heart J., 31(13), 1565-U30 (2010).

[30] Wensing, P. J. W., L. Meiss, W. P. T. M. Mali, *et al.*, "Early atherosclerotic lesions spiraling through the femoral artery", Arterioscler. Thromb. Vasc., 18(10), 1554-1558 (1998).

[31] Salenius, J. P., J. F. Brennan, A. Miller, *et al.*, "Biochemical composition of human peripheral arteries examined with near-infrared Raman spectroscopy", J. Vasc. Surg., 27, 710-719 (1998).

[32] Romer, T. J., J. F. Brennan, M. Fitzmaurice, *et al.*, "Histopathology of human coronary atherosclerosis by quantifying its chemical composition with Raman spectroscopy", Circulation, 97, 878-885 (1998).

[33] Nogueira, G. V., L. Silveira, A. A. Martin, *et al.*, "Raman spectroscopy study of atherosclerosis in human carotid artery",J Biomed Optics, 10, 031117 (2005).

[34] Zinin, P. V., A. Misra, L. Kamemoto, *et al.*, "Visible, near-infrared, and ultraviolet laser-excited Raman spectroscopy of the monocytes/macrophages (U937) cells", J. Raman Spectrosc., 41(3), 268-274 (2010).

[35] Silveira, L., G. V. Nogueira, A. A. Martin, *et al.*, "Raman spectroscopy study of atherosclerosis in human carotid artery", J. Biomed. Optics, 10(3), (2005).

[36] Manoharan, R., J. J. Baraga, M. S. Feld, *et al.*, "Quantitative histochemical analysis of human artery using Raman-spectroscopy", J. Photochem. Photobiol. B, 16(2), 211-233 (1992).

[37] Uchida, Y., Y. Uchida, S. Kawai, *et al.*, "Detection of vulnerable coronary plaques by color fluorescent angioscopy", JACC-Cardiovasc. Imag., 3(4), 398-408 (2010).
[38] Sadler, J. E., "Biochemistry and genetics of von Willebrand factor", Ann. Rev. Biochem., 67, 395-424 (1998).
[39] Ando, J., K. Fujita, N. I. Smith, and S. Kawata, "Dynamic SERS imaging of cellular transport pathways with endocytosed gold nanoparticles", Nano Letts., 11, 5344-5348 (2011).
[40] Faiman, R., "Raman spectroscopic studies of different forms of cholesterol and its derivatives in the crystalline state", Chem. Phys. Lipids, 18, 1, 84 (1977).
[41] Kamemoto, L. E., A. K. Misra, S. K. Sharma, M. T. Goodman, H. Luk, A. C. Dykes, and T. Acosta, "Near-infrared micro-Raman spectroscopy for *in vitro* detection of cervical cancer", Appl. Spectrosc., 64, 255-261 (2010).
[42] Karatas, O. F., E. Sezgin, O. Aydin, and M. Culha, "Interaction of gold nanoparticles with mitochondria", Colloid Surfaces, 71, 315-318 (2009).
[43] Matthews, Q., A. Jirasek, J. Lum, X. B. Duan, and A. G. Brolo, "Variability in Raman spectra of single human tumor cells cultured in vitro: correlation with cell cycle and culture confluency", Appl. Spectrosc., 64, 8, 871-887 (2010).
[44] Pisoni, R. L., "Characterization of a phosphate transport system in human fibroblast lysosomes", J Biol. Chem., 266, 979-985 (1991).
[45] Shamsaie, A., M. Jonczyk, J. Sturgis, J. P. Robinson, and J. Irudayaraj, "Intracellularly grown gold nanoparticles as potential surface-enhanced Raman scattering probes", J. Biomed. Optics, 12, 020502/1- 020502/3 (2007).
[46] Snyder, R. G., S. L. Hsu and S. Krimm, "Vibrational spectra in the C-H stretching region and the structure of the polymethylene chain", Spectrochim. Acta A, 34(4), 395-406 (1978).
[47] Suhalim, J. L., C. Chung, M. B. Lilledahl, R. S. Lim, M. Levi, B. J. Tromberg, and E. O. Potma, "Characterization of cholesterol crystals in atherosclerotic plaques using stimulated Raman scattering and second-harmonic generation microscopy", Biophys. J., 102, 1988-1995 (2012).
[48] Willets, K. A., "Surface-enhanced Raman scattering (SERS) for probing internal cellular structure and dynamics", Anal. Bioanal. Chem., 394, 1, 85-94 (2009).
[49] Matthews, Q., A. Jirasek, J. Lum, X. Duan, and A. Brolo, "Variability in Raman spectra of single human tumor cells cultured in vitero: correlation with cell cycle and culture confluency", Appl Spectrosc, 64, 871-887 (2010).
[50] Movasaghi, Z., S. Rehman, and I. U. Rehman, "Raman spectroscopy of biological tissues", Appl. Spectrosc. Reviews, 42, 493-541 (2007).
[51] Takai, Y., T. Masukp, and H. Takeuchi, "Lipid structure of cytotoxic granules in living human killer T lymphocytes studies by Raman microscopy", Biochem. Biophys. Acta, 1335, 199-208 (1997).

Appendices I-V

UNIVERSITY OF HAWAI'I

Committee on Human Studies

MEMORANDUM

October 18, 2010

TO: Shiv Sharma, Ph.D.
Principal Investigator
Hawaii Institute of Geophysics & Planetology

FROM: Nancy R. King
Director

SUBJECT: CHS #18525- "Biomedical Applications of Micro-Raman and Suface-Enhanced Raman Scattering (SERS) Technology"

Under an expedited review procedure, the research project identified above was approved for one year on October 15, 2010 by the University of Hawaii (UH) Committee on Human Studies (CHS). The application qualified for expedited review under CFR 46.110 and 21 CFR 56.110, Category (2).

This memorandum is your record of CHS approval of this study. Please maintain it with your study records.

CHS approval for this project will expire on October 14, 2011. If you expect your project to continue beyond this date, you must submit an application for renewal of this CHS approval. CHS approval must be maintained for the entire term of your project.

If, during the course of your project, you intend to make changes to this study, you must obtain CHS approval prior to implementing them. Unanticipated problems that are likely to affect study participants must be promptly reported to the CHS.

You are required to maintain complete records pertaining to the use of humans as participants in your research. This includes all information or materials conveyed to and received from participants as well as signed consent forms, data, analyses, and results. These records must be maintained for at least three years following project completion or termination, and they are subject to inspection and review by CHS and other authorized agencies.

Please notify this office when your project is complete. Upon notification, we will close our files pertaining to your project. Reactivation of CHS approval will require a new CHS application.

Please contact this office if you have any questions or require assistance. We appreciate your cooperation, and wish you success with your research.

1960 East-West Road, Biomedical B104, Honolulu, Hawaii 96822-2303
Telephone: (808) 956-5007, Facsimile: (808) 956-8683, Website: www.hawaii.edu/irb

UNIVERSITY OF HAWAI'I
Committee on Human Studies

MEMORANDUM

August 26, 2011

TO: Shiv K. Sharma, Ph.D.
Principal Investigator
Hawaii Institute of Geophysics & Planeology

FROM: Nancy R. King
Director

SUBJECT: CHS #18525- "Biomedical Applications of Micro-Raman and Surface-Enhanced Raman Scattering (SERS)"

Under an expedited review procedure, the research project identified above was approved for one year on August 25, 2011 by the University of Hawaii (UH) Committee on Human Studies (CHS). The application qualified for expedited review under CFR 46.110 and 21 CFR 56.110, Category (2).

This memorandum is your record of CHS approval of this study. Please maintain it with your study records.

CHS approval for this project will expire on August 24, 2012. If you expect your project to continue beyond this date, you must submit an application for renewal of this CHS approval. CHS approval must be maintained for the entire term of your project.

If, during the course of your project, you intend to make changes to this study, you must obtain CHS approval prior to implementing them. Unanticipated problems that are likely to affect study participants must be promptly reported to the CHS.

You are required to maintain complete records pertaining to the use of humans as participants in your research. This includes all information or materials conveyed to and received from participants as well as signed consent forms, data, analyses, and results. These records must be maintained for at least three years following project completion or termination, and they are subject to inspection and review by CHS and other authorized agencies.

Please notify this office when your project is complete. Upon notification, we will close our files pertaining to your project. Reactivation of CHS approval will require a new CHS application.

Please contact this office if you have any questions or require assistance. We appreciate your cooperation, and wish you success with your research.

1960 East-West Road, Biomedical B104, Honolulu, Hawaii 96822-2303
Telephone: (808) 956-5007, Facsimile: (808) 956-8683, Website: www.hawaii.edu/irb

Office of Research Compliance
Human Studies Program

UNIVERSITY of HAWAI'I® MĀNOA

MEMORANDUM

July 19, 2012

TO: Shiv Sharma, Ph.D.
Principal Investigator
Hawaii Institute of Geophysics and Planetology

FROM: Ching Yuan Hu, Ph.D.
Interim Director
Human Studies Program
Office of Research Compliance
University of Hawaii, Manoa

SUBJECT: CHS #18525- "Biomedical Applications of Micro-Raman and Surface-Enhanced Raman Scattering (SERS) Technology"

Under an expedited review procedure, the research project identified above was approved for one year on July 18, 2012 by the University of Hawaii (UH) Human Studies Program. The application qualified for expedited review under CFR 46.110 and 21 CFR 56.110, Category (8b).

This memorandum is your record of the Human Studies Program approval of this study. Please maintain it with your study records.

The Human Studies Program approval for this project will expire on July 17, 2013. If you expect your project to continue beyond this date, you must submit an application for renewal of this Human Studies Program approval. The Human Studies Program approval must be maintained for the entire term of your project.

If, during the course of your project, you intend to make changes to this study, you must obtain the Human Studies Program approval prior to implementing them. Unanticipated problems that are likely to affect study participants must be promptly reported to the Human Studies Program.

You are required to maintain complete records pertaining to the use of humans as participants in your research. This includes all information or materials conveyed to and received from participants as well as signed consent forms, data, analyses, and results. These records must be maintained for at least three years following project completion or termination, and they are subject to inspection and review by the Human Studies Program and other authorized agencies.

1960 East-West Road
Biomedical Sciences Building B104
Honolulu, Hawai'i 96822
Telephone: (808) 956-5007
Fax: (808) 956-8683

Please notify this office when your project is complete. Upon notification, we will close our files pertaining to your project. Reactivation of the Human Studies Program approval will require a new Human Studies Program application.

Please contact this office if you have any questions or require assistance. We appreciate your cooperation, and wish you success with your research.

UNIVERSITY OF HAWAI'I AT MĀNOA

School of Ocean and Earth Science and Technology
Hawai'i Institute of Geophysics and Planetology

Office of the Director

August 12th, 2011

Dr. Jeffrey L. Berenberg
Principal Investigator
Hematologist-Oncology Service
MCHK-DMO, TAMC
1 Jarrett White Road
Honolulu, Hawaii 96859-5000

Dear Dr. Berenberg:

I am pleased to provide this letter of support for your research project, "*Biomedical Applications of Micro-Raman and Surface-Enhanced Raman Scattering (SERS) Technology.*" Our modern research facilities here at the Hawaii Institute of Geophysics and Planetology (HIGP) support a great variety of projects. Prominent among our research assets is the Raman Spectroscopy Laboratory. This Facility occupies approximately 1920 ft^2 of contiguous laboratory space in the Hawaii Institute of Geophysics (HIG) building. Micro-Raman spectroscopy instrumentation in BSL2 laboratory occupies ~960 ft^2 of space. The rest of the space is dedicated for development of remote Raman, fluorescence and laser induced break-down spectroscopy related research activities. This Facility has been upgraded to a Bio Safety Level 2 (BSL2) Raman Facility to facilitate measurements of Raman spectra of biomedical samples including biological cells, various types of tissues, body fluids, bacteria and viruses.

In addition to the Raman Facility, a dedicated BSL 2 Microbiology Research Laboratory (364 ft^2) was established in the HIG building in support of biomedical research. This laboratory houses equipment essential in the handling of biological samples. A partial listing notes the use of a Fisher Scientific Ultra-low Temperature upright freezer (-80°C); the Torr International thin film thermal evaporation system, used for metal deposition onto substrates of interest for surface enhanced Raman scattering (SERS) spectroscopy; a ThermoScientific Biosafety cabinet; a HERAcell 150 CO_2 incubator; and a Fisher Scientific Micromaster inverted microscope.

I believe that HIGP's resources are ideal to support your efforts to investigate the biomedical applications of Raman spectroscopy. I look forward to hearing your progress in this endeavor.

Sincerely,

Pete Mouginis-Mark
Director, HIGP

1680 East-West Road, POST 602, Honolulu, Hawai'i 96822 USA
Telephone: (808) 956-8760, Facsimile: (808) 956-3188

Appendix III: E-mail from Dr. Berenberg Regarding Approval of the Protocol

Shiv Sharma <shiv@hawaii.edu>

IRBNet message from Sharon Esser (UNCLASSIFIED)

2 messages

Berenberg, Jeffrey L COL MIL USA MEDCOM TAMC <jeff.berenberg@us.army.mil> Sun, Oct 14, 2012 at 11:08 AM
To: Shiv Sharma <shiv@hawaii.edu>, "Hoover, Christine D Ms CIV USA MEDCOM TAMC" <Christine.D.Hoover@us.army.mil>, "Andrews, Barbara A Ms CIV USA MEDCOM TAMC" <Barbara.Andrews1@us.army.mil>

Classification: UNCLASSIFIED
Caveats: NONE

Hi Shiv

How should we proceed now? Thanks Jeff

-----Original Message-----
From: Sharon Esser [mailto:dmrn_no_reply@dmrn.dhhq.health.mil]
Sent: Friday, October 12, 2012 2:37 PM
To: Berenberg, Jeffrey L COL MIL USA MEDCOM TAMC; Andrews, Barbara A Ms CIV USA MEDCOM TAMC; Nakano, Eileen T Dr CTR US USA MEDCOM TAMC; Mimaki, Carroll H Mr CTR US USA MEDCOM TAMC; Garshnek, Victoria CIV US USA MEDCOM TAMC
Subject: IRBNet message from Sharon Esser

Message from Sharon Esser:

Re: [367816-2] Biomedical Applications of Micro-Raman and Surface-Enhanced Raman Scattering (SERS) Technology

Dr. Berenberg,

Your protocol has been forwarded via IRBNet to CIRO to be reviewed in coordination with the CRADA, previously submitted to CRADA by Dr. Eileen Nakano. Your start letter and start book are ready for you to pick up at your convenience at the DCI. Please note that although your protocol is approved, you are not approved to initiate any CRADA related research activities until you receive a separate CRADA approval. Please call Dr. Garshnek at 433-7171 to arrange for a brief meeting at the DCI to pick up your start letter.

Regards,

Sharon Esser

For additional support please visit the DMRN resource center at
https://www.us.army.mil/suite/page/596540

Classification: UNCLASSIFIED
Caveats: NONE

Shiv Sharma <shiv@hawaii.edu> Sun, Oct 14, 2012 at 12:17 PM
To: "Berenberg, Jeffrey L COL MIL USA MEDCOM TAMC" <jeff.berenberg@us.army.mil>
Cc: "Hoover, Christine D Ms CIV USA MEDCOM TAMC" <Christine.D.Hoover@us.army.mil>, "Andrews, Barbara A Ms CIV USA MEDCOM TAMC" <Barbara.Andrews1@us.army.mil>

Dear Dr. Berenberg,

Thanks a lot for your e-mail. It is good news to hear that your protocol is approved. You still have to receive a separate CRADA approval before we could initiate research work on clinical samples. We are approaching close to finally get the paperwork in place! Please follow the instructions in Sharon's e-mail to pick up the documents on CRADA and e-mail to me a copy so that I could submit the documents to UH ORS, and include in our 8th quarterly report and final report for the project.

At our end, I have requested our Director to provide funding for continuing work on the project for the month of November and December 2012 as our current contact end on 29th of October 2012. We are currently looking at the micro-Raman spectra of exfoliated normal cells from urine of healthy volunteers to establish the protocol. Once we have all the paperwork in place, we may like to consider applying for a grant to continue our proposed clinical work.

With regards and best wishes,

Shiv

[Quoted text hidden]

--
Professor Shiv K. Sharma
Hawaii Institute of Geophysic & Planetology
University of Hawaii
1680 East-West Road, POST #602
Honolulu, HI-96822
USA

Phone: (808) 956-8476
Fax: (808) 956-3188

Appendix IV: Reprint Proceedings SPIE 8035, 802503/1-802503/11 (2011)

Nitrocellulose-based SERS immunosensor for detection of biological molecules

A. C. Dykes[a], L. Kamemoto[a,b], A.K. Misra[a], and S. K. Sharma[a]
[a]University of Hawaii, Hawaii Institute for Geophysics and Planetology, 1680 East-West Rd., POST #602, Honolulu, Hawaii 96822
[b]University of Hawaii, John A. Burns School of Medicine, 1319 Punahou Street, Suite 824, Honolulu, Hawaii 96826

ABSTRACT

We have developed a simple and potentially a low-cost method for the sensitive detection of target proteins via surface-enhanced Raman scattering (SERS). The immunosensor constructed by the conjugation of monoclonal antibodies to 20 nm diameter gold nanoparticles via the bifunctional Raman reporter molecule, 5, 5′-dithiobis (succinimidyl-2-nitrobenzoate) (DSNB) is the basis of a membrane-bound detection system. Traditionally, a common laboratory technique called a dot blot, which is a colorimetric method where detection of proteins is accomplished through the application of assorted dyes followed by their measurement via a densitometer. Dot blotting is a convenient and time saving method that involves the spotting of a protein onto an immobilizing matrix, such as nitrocellulose (NC) or polyvinylidene fluoride (PVDF) membrane. We found that for detection via SERS spectroscopy NC is the matrix of choice because it offers low background, minimal preparation prior to protein application, and optimal position of Raman bands. Furthermore, SERS detection of protein on NC requires only minimal sample preparation and demonstrates increased sensitivity when compared to other dot blot detection methods. Depending on the dye used for visualization, dot blots analyzed by commonly used optical methods have limits of detection in the nanogram range, some as low as 20 pg/ml. Here we demonstrate the use of the dot blot method for detecting target proteins (e.g., protein A and prostate specific protein (PSA)) by SERS spectroscopy down to a concentration of 100 fg/ml.

KEYWORDS: surface-enhanced Raman scattering (SERS); Raman reporter-labeled immunogold colloids; SERS-immunosensor; nitrocellulose; protein A; prostate-specific antigen (PSA)

1. INTRODUCTION

Until recently, Raman spectroscopy lacked the sensitivity needed for use as a readout method. Current advancements in surface-enhanced Raman scattering (SERS) detection have led to the incorporation of this technique into the immunoassay format. SERS is a surface sensitive occurrence that results in the 10^{14}-10^{15} enhancement of Raman scattering by analyte molecules adsorbed on the rough surfaces of coinage (Au, Ag, Cu) or alkali (Na, K, Li) metals.[1] SERS spectroscopy is thought to be the result of two contributing effects: chemical and electromagnetic.[2] The chemical mechanism is associated with a charge transfer process between an adsorbed analyte and a metal surface. Essentially, vibrations involved in the charge transfer process are enhanced, a phenomenon similar to resonant enhancement.[3] Enhancement produced by this component is in 10-10^3 range.[1] The dominant electromagnetic contribution is due to an electromagnetic field enhancement caused by plasmon excitation through incident laser light on the metal surface. Electrons in the metal are excited to an oscillation in the metal cores, called a surface plasmon. Because the plasmon excitation is dependent on incident light, the excitation for a SERS experiment would ideally be adapted to the plasmon wavelength of the surface metal, which also affects the plasmon resonance wavelength.[3] Advantages of using SERS as a readout method versus fluorescence include the fact that Raman labels have narrow lines, which minimizes the potential for spectral overlap when more than one label is involved. Secondly, Raman labels are not as prone to photobleaching as fluorescence at laser powers typically used for sample evaluation, allowing for greater signal-to-noise ratio through longer collection times. Lastly, there are fewer limitations concerning the excitation wavelength for Raman labels. Raman spectra are molecule specific. The narrow Raman bands are recorded as Raman shifts (in cm^{-1}) with respect to the excitation wavelength and Raman spectral features do not change with changing excitation wavelength. Additionally, spectra f rom multiple Raman labels excited by a single wavelength can beinterpreted with less difficulty than the emission of multiple fluorophores in most instances.[4]

*Corresponding Author: E-mail: sksharma@soest.hawaii.edu; phone 808-956-8476

Smart Biomedical and Physiological Sensor Technology VIII, edited by Brian M. Cullum, Eric S. McLamore,
Proc. of SPIE Vol. 8025, 802503 · © 2011 SPIE · CCC code: 1605-7422/11/$18 ·
doi: 10.1117/12.884369

Grubisha et al.[5] have successfully utilized SERS with the sandwich immunoassay. They employed monoclonal antibodies to prostate-specific antigen (PSA) coupled to Raman reporter-coated gold nanoparticles (AuNPs); PSA could be detected in a serum matrix down to 1 pg/ml. The Raman peak resulting from the symmetric nitro stretch of the bifunctional reporter 5, 5'-dithiobis (succinimidyl-2-nitrobenzoate) (DSNB) was monitored while measuring samples containing a range of concentrations of PSA. While a limit of detection (LOD) of 1 pg/ml is well within the normal limits of PSA levels in a normal healthy male, the ability to monitor even lower levels may prove beneficial in following prostate cancer patients.

In the United States, prostate cancer is the second leading cause of cancer deaths in men.[6] Because there is currently no cure for locally advanced or metastatic prostate cancer, early detection and treatment are essential for a favorable prognosis. PSA is a serine protease whose functions in the seminal fluid are the liquefaction of semen and the dissolution of the cervical mucus cap, which allows for the entry of sperm into the cervix for fertilization. PSA is released into the blood of healthy males at low concentrations. In males afflicted with prostate cancer, PSA levels are increased and can be correlated with tumor volume and tissue specificity. Although routine PSA screening has resulted in 90% of all prostate cancers being diagnosed at an early, treatable stage[7], the PSA assay finds its greatest utility as a prognostic indicator of prostate cancer recurrence. Studies have shown that serial evaluation of PSA levels post-prostate cancer treatment is effective in indentifying recurrence or further metastasis.[8]

Another laboratory test where SERS can be a useful readout method is a variation of the immunoassay called the dot blot.[9-11] Traditionally a dot blot is a colorimetric method where the detection of these proteins is accomplished through the application of assorted dyes followed by their measurement via a densitometer.[12] A convenient and timesaving method, dot blotting involves the spotting of a protein onto an immobilizing matrix, such as nitrocellulose (NC) or polyvinylidene fluoride (PVDF) membrane. We found that for detection via SERS spectroscopy NC is the matrix of choice because it offers low background, minimal preparation prior to protein application, and optimal position of Raman bands. Furthermore, it does not require any additional sample preparation and offers increased sensitivity to other detection methods. Depending on the dye used for visualization dot blots analyzed by optical methods have limits of detection in the nanogram range, some as low as 20pg/ml.[8,9,13] Here we demonstrate the use of the dot blot method for detecting antigens (e.g., protein A (PA) and prostate-specific antigen (PSA)) by SERS spectroscopy down to a concentration of 100fg/ml.

Protein A is a cell wall protein produced by *Staphylococcus aureus* (*S. aureus*), a pathogenic bacterium that causes human infection. The detection of this bacterium via PA recognition in processed foods can be important in clinical diagnosis.[13] A 43 kDa protein, PA can selectively bind the fragment crystallizable (Fc) region of immunoglobulin G (IgG) at sites other than the antigen's binding site, making it a useful tool for immunosensing applications and the laboratory isolation and purification of antibody molecules.[13,14] An array of biological functions has been associated with PA as well. Besides having antitumor, anticarcinogenic, and antitoxic effects, PA also has immunomodulatory, antifungal, and antiparasitic properties. PA has also been shown to act as a B and T cell mitogen and induce the production of different cytokines such as TNFα and IL-1α.[14,15]

The detection of our target proteins, PSA and PA, has important implications but the inherent advantage of the antibody-DSNB-AuNP reporter system is its versatility. By coupling an appropriate antibody with the AuNP-DSNB complex, an immunosensor could be constructed with the ability to detect any protein to which an antibody is available. While in each of these cases the specificity of the sensor would be related to the properties of the antibody, the sensitivity will rely more heavily on the properties of the SERS-based Raman sensor.

2. METHODOLOGY

2.1 Chemicals

Protein A and monoclonal anti-protein A antibody were purchased from Sigma Aldrich (St. Louis, MO, USA). Antibodies to PSA were received from Fitzgerald Industries (Concord, MA, USA), while the PSA antigen was purchased from Bios Pacific (Emeryville, CA, USA). ImmunoPure normal human serum was acquired from Pierce Biotechnology (Rockford, IL, USA). Unless otherwise stated, all other reagents were used as received from Sigma Aldrich (St. Louis, MO, USA).

2.2 Gold nanoparticle (AuNP) preparation

Gold colloids were made by adding 1 ml of 1% hydrogen tetrachloroaurate (III) ($HAuCl_4$) to 100 ml of distilled water, followed by 2 ml of 1% sodium citrate tribasic dihydrate ($Na_3C_6H_5O_7$). Approximately 1 ml of 0.1M K_2CO_3 was added to adjust the pH to 7.[16] The solution was heated under reflux for 20 to 30 minutes, until the color turned a deep purple. Evaluation by photon correlation spectroscopy revealed that particle size was approximately 20 nm. The concentration of AuNPs in the solution was calculated to be 9.23×10^{11} particles/ml.

2.3 DSNB synthesis

Synthesis of DSNB was carried out as previously described[5] Briefly, 0.50 g of 5, 5′-dithiobis (2-nitrobenzoic acid) (DNBA), 0.52 g of 1, 3-dicyclohexylcarbodiimide (DCCD), and 0.29 g of *N*-hydroxysuccinimide (NHS) were sequentially added to 50 ml tetrahydrofuran in a 500 ml round-bottom flask equipped with a drying tube. After stirring for 24 hours at room temperature, the solution was filtered and then rotoevaporated to remove solvent. The product was recrystallized as a yellow powder with acetone/hexane solvent.

2.4 Preparation of DSNB-labeled immunogold colloids

DSNB-labeled SERS reporters were made by adding 100 µl of 2.5mM DSNB in acetonitrile to 1 ml of unconjugated gold sol and allowing the reaction to proceed for 4 to 8 hours. The mixture was then centrifuged at 10,000 *g* for 7 minutes. The clear supernatant was discarded and the loose sediment was resuspended in 1 ml borate buffer (2 mM, pH 9). Next, 35 µg of detection antibody (4.2 µl of an 8.3 mg/ml anti-protein A clone SPA-27 solution or 14.3 µl of a 2.45 mg/ml PSA-66 solution) was added. This mixture was incubated at room temperature for 1 hour. After a second centrifugation and removal of the supernatant, the precipitate was resuspended in 1 ml of 2mM Tris buffer (pH 7.6) with 1% bovine serum albumin (BSA).

Figure 1(A) demonstrates the basic reaction between DSNB and a single gold nanoparticle. The interaction of DSNB with the gold surface results in AuNP coated with a thiolate of DSNB. The intermediate species formed is a Raman-reporter-labeled AuNP containing a reactive group, R ($C_5H_5NO_3$). This Raman reporter molecule can then react with the primary amine of an antibody by forming an amide linkage[5] creating a bifunctional Raman reporter. Figure 1(B) depicts how multiple reporters may interact with a single AuNP. The presence of the reactive groups allow for the coupling of the antibody at the distal end of the reporter. Monofunctional reporters position antibodies alongside the reporters, where they would be competing for available space. A monofunctional reporter such as this would accommodate fewer antibody molecules, allowing for the attachment of fewer antigens. Additionally, the monofunctional configuration would permit a smaller number of reporters per AuNP, resulting in decreased signal from each reporter construct.

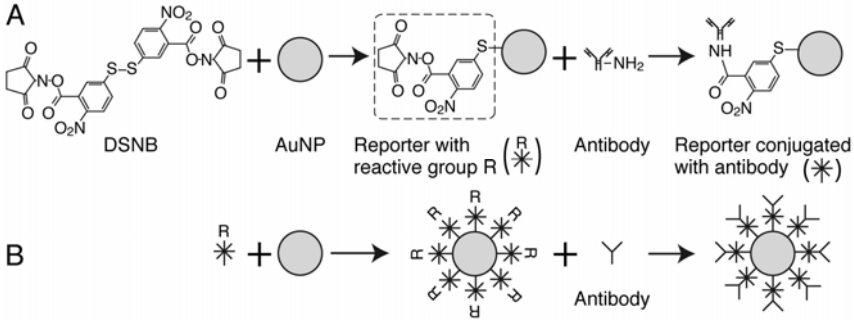

Figure 1. (A) Conjugation chemistry of DSNB molecule with AuNPs. Exposure of DSNB to the gold surface yields an AuNP coated with the thiolate of DSNB. The thiolate contains a reactive group that then forms an amide linkage with the primary amine of an antibody. (B) Schematic representation of AuNP-antibody orientation following reaction with DSNB. The bifunctional nature of this reporter allows for a greater number of reporters to be associated with each AuNP and a matching number of antibodies can, in turn, be associated with each reporter.

2.5 Preparation of modified dot blot

A 3×4 grid was drawn on a 3″×3″ square of nitrocellulose membrane using a pencil. Five µl of protein A or PSA diluted in phosphate-buffered saline (PBS, pH 7.5) ranging from concentrations of 0 to 10µg were pipetted to the center of each square. After drying, the membrane was pre-wet with a solution of 0.5% Tween 20 in phosphate-buffered saline (PBS-T). The SNAP i.d. protein detection system (Millipore Corporation, Billerica, MA) was used for blocking and antibody

introduction to the membrane. After placing the membrane in the blot holder, it was positioned in the SNAP i.d. system. Thirty milliliters of SuperBlock T20 blocking buffer were poured into the blot holder and allowed to incubate for 10 minutes. Vacuum was applied to system until the blot holder well was completely empty. Next, 3 ml of the anti-PSA- or anti-protein A-DSNB-labeled gold nanoparticles were placed in the well and allowed to incubate for 10 minutes. Vacuum was applied to pull the antibody solution through the membrane then left on during three consecutive rinses with PBS-T. The blot was removed from the holder and allowed to air dry. It was then affixed to an aluminum block with double-sided tape in preparation for evaluation with micro-Raman spectroscopy.

2.6 UV-visible spectroscopy

UV-visible spectroscopy scans were conducted using an Evolution 60 spectrophotometer (Thermo Scientific, Madison, WI, USA) equipped with a xenon light source. Gold nanoparticles were evaluated by scanning 450 to 1000 nm in absorbance mode with a wavelength interval of 1 nm.

2.7 Micro-Raman spectroscopy

All SERS spectra were excited by an Invictus 785-nm NIR laser and measured with a fiber-coupled micro-*Raman RXN system* (Kaiser Optical Systems, Inc., Ann Arbor, MI) equipped with 50-micron slit. The micro-Raman system uses a 785 nm CW laser and CCD detector. A 10× objective (NA 0.25) that produced a 75 μm laser spot size on the sample was used for all measurements. The Rayleigh scattered laser radiation was rejected by utilizing a 785 nm notch filter. The cosmic rays were removed using software provided by Kaiser optical system, which measures the spectra twice and deletes the random peaks due to cosmic rays.

3. RESULTS AND DISCUSSION

3.1 Evaluation of SERS activity of AuNPs

Figure 2 shows the absorbance spectra for a series of AuNP solutions of differing pH values prepared under otherwise identical conditions in our laboratory. Only those AuNPs prepared at pH 7.0 display a large absorbance in the NIR region. The deep purple hue of our AuNP preparation correlates with this finding and is proof of aggregate formation.[17] Rather than the red color characteristic of a single particle plasmon region, this Au solution more strongly absorbs and scatters light over a broad band of longer wavelengths and appears purple.[18]

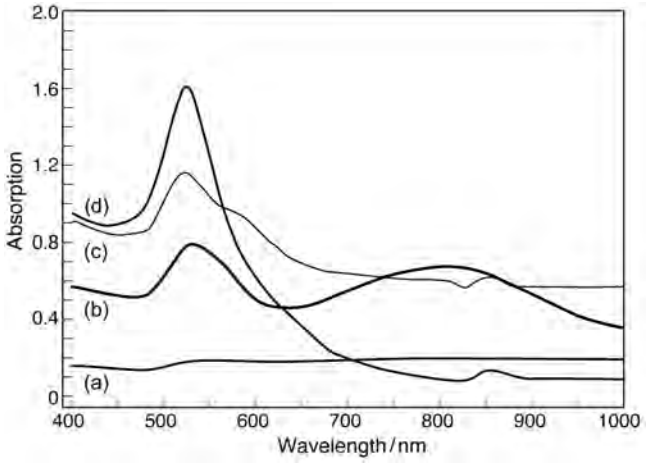

Figure 2. Absorbance spectra of gold sols prepared at a range of pH values: (a) pH 6.0; (b) pH 7.0; (c) pH 8.0; and (d) pH 9.0. Spectral curves have been displaced vertically for clarity.

Evaluation by photon correlation spectroscopy of gold sol revealed particle size to be approximately 20 nm. The concentration of AuNPs in the solution was calculated to be 9.23×10^{11} particles/ml. At pH 7 the gold sol aggregates show a broad absorption band in the near infrared at ~800 nm in addition to the Au nanoparticles absorption band at 529 nm. This NIR band is believed to originate from the surface plasmon resonance of aggregated gold particles.

The efficacy of AuNPs was evaluated using the well-characterized Raman reporter rhodamine 6G (R6G) solutions. Notable Raman bands associated with this molecule include 615 cm^{-1} (C-C-C in-plane bend); 775 cm^{-1} (C-H out-of-

plane bend); 1363 cm^{-1} (aromatic C-C stretch); and 1509 cm^{-1} (aromatic C-C stretch).[19] Figure 3 displays the intensity of each of these peaks as monitored during Raman evaluation of several concentrations of R6G. Methanolic solutions of R6G are readily detectable down to 1 mM both alone and when in combination with commercially available gold nanoparticles. A slight enhancement in signal intensity was observed in the presence of AuNPs and this intensity of the Raman lines tends to increase with decreasing particle size. On the other hand, R6G interaction with AuNPs prepared in-house produce peak intensities several-fold higher than those of R6G alone. R6G could be detected at concentrations down to 10^{-8} M.

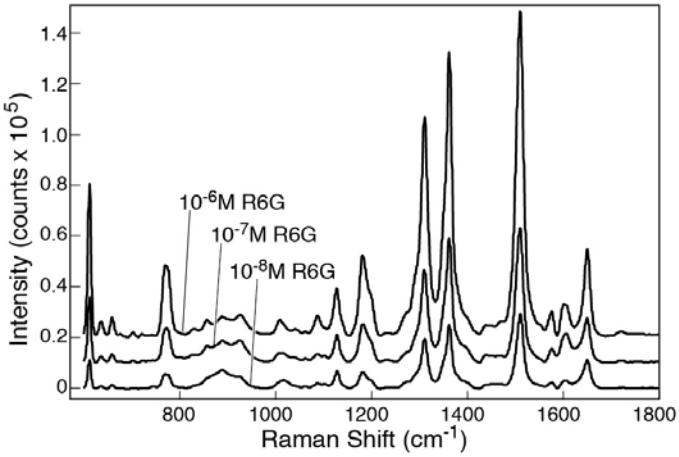

Figure 3. SERS spectra of various concentration of R6G mixed with AuNPs prepared in our laboratory.

A key factor in this improved detection is the production of gold sols in our laboratory. Commercial gold sols are maintained at conditions aimed at keeping the colloids monodispersed. *De novo* synthesis of AuNPs allows greater control over reaction conditions that have substantial effects on the characteristics of the AuNPs. Parameters such as the concentration of reactants, temperature, and the effect of additives contribute to NP size and shape.[20] These properties in turn affect the optical, electronic, magnetic and catalytic properties of the AuNPs.[21] Another useful parameter is the pH of the reactant solution. Patungwasa et al.[20] have shown that NP size decreases with increasing pH. Increasing the pH of our citrate reduction solution to 7.0 also imparts a more uniform spherical shape and narrower size distribution. At this pH the citrate acts as a stabilizing agent that can modulate the aggregation process after the reduction of the $AuCl^{-4}$ ions. This occurs because the average charge of the citrate ions modulates the surface charge of the newly formed AuNPs and allows for greater interaction between them.[20]

Figure 4 exhibits the ability of our AuNPs to aggregate at pH 7.0, in which they are prepared and stored. Line A is the absorption spectra for the AuNPs as prepared. The narrow peak at 520 nm represents the dispersed 20 nm AuNPs, while the broader band centered at 790 nm indicates the presence of large aggregates of AuNPs. Line B in this figure is the spectrum of the AuNPs with the addition of anti-protein A monoclonal antibody. The broadening of each peak towards longer wavelengths indicates the nanoparticles' interaction with the antibody. Line C represents the spectrum of AuNPs, anti-protein A antibody, plus protein A antigen (10 μg/ml). The further broadening of the peaks and the decrease in the overall intensity of the spectrum is the result of complex formation with the addition of the antigen. As discussed below, the AuNP-antibody-antigen complexes yield a much higher degree of surface-enhanced Raman scattering at 785 nm excitation than an equivalent-sized solid AuNP-reporter. Within the complexes are intricate systems of these molecules in contact with AuNPs. Each of these is capable of generating a Raman signal.[22] Studies involving DNA-linked metal nanospheres yielded similar results. Suspensions of Au colloid linked to DNA fragments yielded extinction spectra that were red shifted and broadened as compared to dispersed Au colloid.[18]

3.2 Raman spectra of DSNB powder and solution adsorbed on AuNPs

The Raman spectrum of DSNB powder is shown in Figure 5. The spectrum was collected with laser power of 50 mW at the sample and 10 s of integration time. The laser spot size was 75 μm at the sample. The peaks at 851 cm^{-1} (nitro scissoring vibration), 1079 cm^{-1}(succinimidyl N-C-O stretch overlapping with aromatic ring modes), 1342 cm^{-1} (symmetric nitro stretch), and 1566 cm^{-1} (aromatic ring mode refer to as (8a)) are indicative of the presence of DSNB.[5]

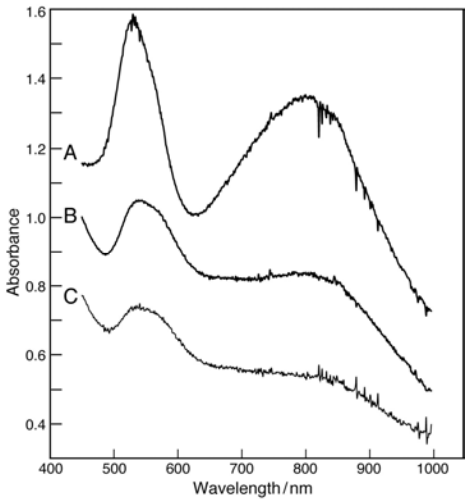

Figure 4. Absorbance spectra of (**A)** AuNPs alone, (**B)** AuNPs plus DSNB reporter plus antibody, and (**C)** AuNPs plus DSNB reporter plus antibody plus antigen. Absorbance in the range of 520 to 550 nm is due to monodispersed gold colloids. The increased absorbance in the area from 600 to 820 nm is due to gold colloid aggregates formed from antibody –antigen interactions. The peak broadened and its intensity diminished as antibody-antigen interactions promote the formation of larger aggregates. Spectral curves are vertically shifted for clarity.

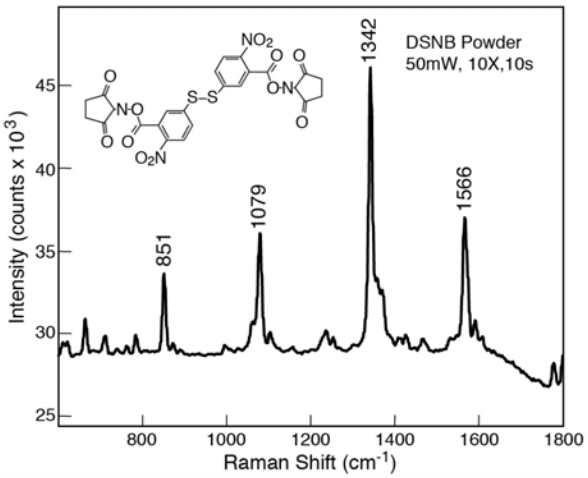

Figure 5. Raman spectrum of yellow DSNB powder. Prominent peaks at 851 cm^{-1} (nitro scissoring vibration), 1079 cm^{-1} (succinimidyl N-C-O stretch overlapping with aromatic ring modes), 1342 cm^{-1} (symmetric nitro stretch), and 1566 cm^{-1} (aromatic ring mode (8a)) are indicated.[5] (785 nm excitation, 50 mW, 10 X objectives, 10 s integration)

The spectrum of DSNB-AuNPs (Fig. 6) varies slightly from that of DSNB powder alone. Once the DSNB is chemisorbed onto the gold surfaces, small shifts occur in the principal peaks of the spectrum. Most notably, the prominent symmetric nitro stretch has shifted to 1338 cm^{-1}. It is the intensity of this peak that is used to quantify the antibody antigen reaction. Other changes include the shift of the succinimidyl N-C-O stretch from 1079 to 1077 cm^{-1} and the aromatic ring mode from 1566 to 1559 cm^{-1}.

3.3 SERS-based protein A sensor

The first reporters constructed were anti-protein A-DSNB-AuNPs. As described above, these probes were used to evaluate a dot blot comprised of a range of protein A concentrations. A typical SERS spectrum of anti-protein DSNB on AuNPs on nitrocellulose membrane is shown in Figure 7.

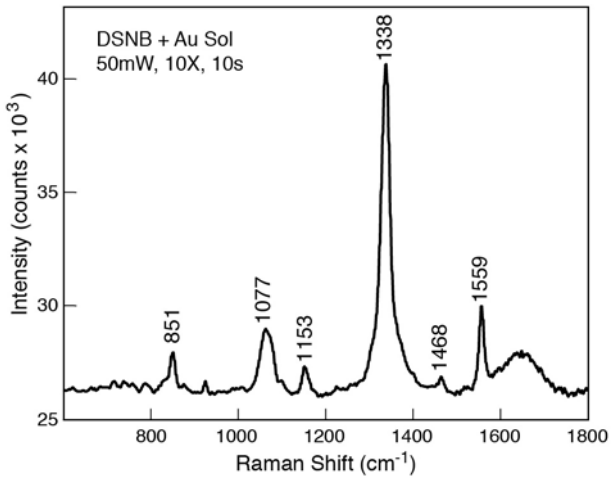

Figure 6. Typical Raman spectrum resulting from DSNB chemisorbed onto AuNPs with 10s integration time and 50 mW of laser power. Prominent bands have undergone a slight shift: 851 cm^{-1} (nitro scissoring vibration), 1077 cm^{-1} (succinimidyl N-C-O stretch overlapping with aromatic ring modes), 1338 cm^{-1} (symmetric nitro stretch), and 1559 cm^{-1} (aromatic ring mode (8a)).[5]

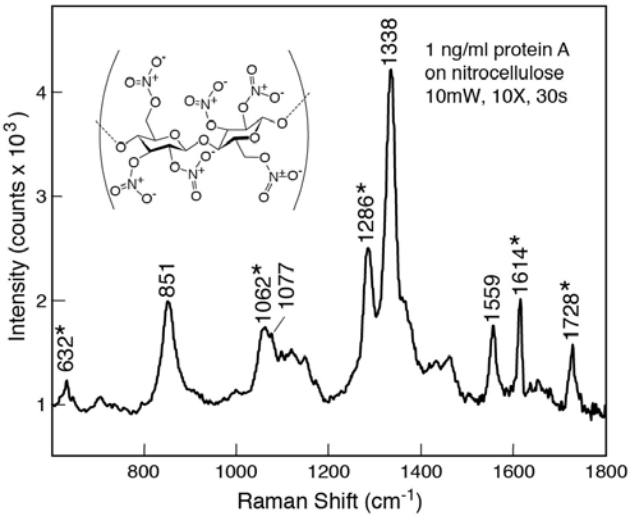

Figure 7. Representative spectrum of anti-protein A-DSNB-AuNP reporters on nitrocellulose membrane. Raman bands from DSNB and nitrocellulose (marked by *) are indicated. Laser power was 15 mW with an integration time of 10 s.

The peaks associated with the DSNB reporter are juxtapositioned with new peaks associated with the nitrocellulose membrane. These peaks do not interfere with the prominent symmetric nitro stretch at 1338 cm^{-1} and so immobilization on nitrocellulose may be a viable alternative as a substrate. The intensity of the signal of the DSNB probes is sufficient for analysis even in the absence of a gold or silver substrate. The results are shown in Figure 8. The normalized intensity of the 1338 cm^{-1} peak is plotted as a function of protein A concentration. Each point is the average of at least five spectra. Quantities of protein A were detectable down to a concentration of 100 fg/ml using this method. Concentrations below this limit were not statistically significant from blank samples (containing no protein A).

3.4 SERS-based prostate specific antigen sensor

In the same manner as described above, Anti-PSA-DSBN-AuNPs were used in the assembly of a PSA dot blot assay. The results are summarized in Figures 9 and 10. Figure 9 shows the resultant spectra for PSA concentrations from 100 fg/ml to 10^6 fg/ml. A plot of the intensity of the peak at 1338 cm^{-1} yields the graph in Figure 10. Each point represents the average of the intensity of this peak from 10 different spectra. Note PSA concentrations of 10^3, 10^6 and 10^9 fg/ml

correspond to 1 pg/ml, 1 ng/ml and 1 μg/ml, respectively. Because the intensities associated with 1 and 10 fg/ml concentrations were not significantly different from zero, the LOD for this assay was found to be 100 fg/ml.

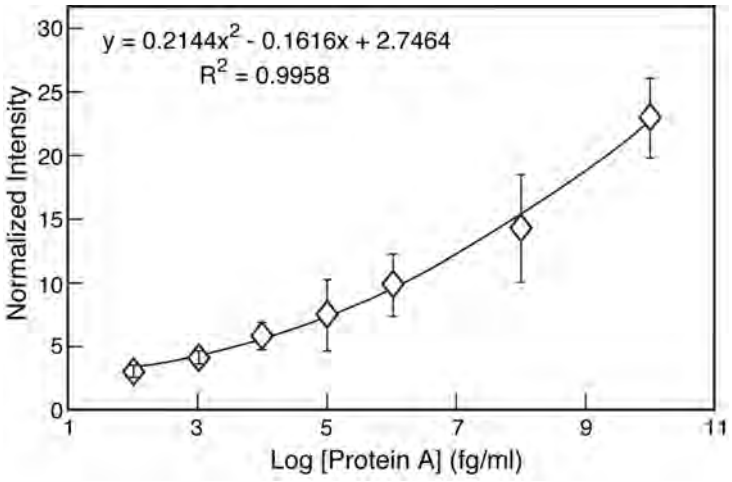

Figure 8. Plot of log protein A concentration (fg/ml) versus integrated intensity at Raman peak located at 1338 cm^{-1} normalized by peak intensity at 632 cm^{-1}. Concentrations ranged from 100fg/ml to 10 μg/ml.

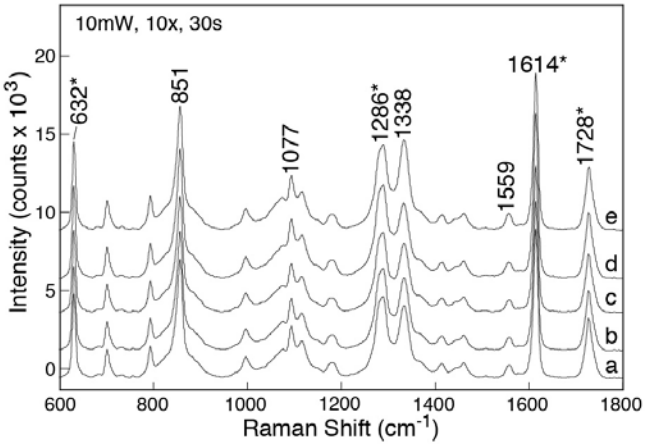

Figure 9. SERS spectra of PSA dot blot assay acquired at PSA concentrations of (a) 10^2, (b) 10^3(c) 10^4, (d) 10^5 and (e) 10^6 fg/ml, respectively. Each spectrum was measured with 10 mW of laser power and 30 s integration time. The bands due to nitrocellulose membrane are marked by asterisks (*).

PSA assays currently in clinical use are typically a double monoclonal antibody sandwich reaction with electrochemiluminescent or fluorescent detection. These technologies have a sensitivity of about 0.1ng/ml. Lower values typically cannot be distinguished from zero and are reported as < 0.1ng/ml.[23] Although this LOD is adequate for an initial evaluation for the presence of prostate cancer (PC), patients who have been treated for PC by undergoing radical prostatectomy (RP) will have very low to zero PSA in the blood. Monitoring PSA levels with lower LOD in these patients can be effective in indentifying recurrence or further metastasis earlier than previously possible.[8] Because PSA elevations in serum occur earlier than the development of clinical symptoms, PSA-defined biochemical relapse is now widely accepted as an early indicator of tumor recurrence.[24] The development of detection methods such as the SERS-based immunoassay that are capable of measuring PSA below the current detectable limit could lead to earlier detection and treatment of recurrent prostate cancer, enabling earlier relapse detection and intervention.

As described above, the increased sensitivity observed in these studies is due in part to the characteristics of the DSNB-labeled AuNPs. The orientation of the DSNB reporter, as illustrated in Figure 1, allows for a maximum number of reporter molecules per nanosphere. Smaller sphere diameter allows for greater surface area in a comparable volume.

This effect is enhanced by the aggregation of the AuNPs into large clusters whose maximum absorption occurs at the excitation wavelength 785nm.

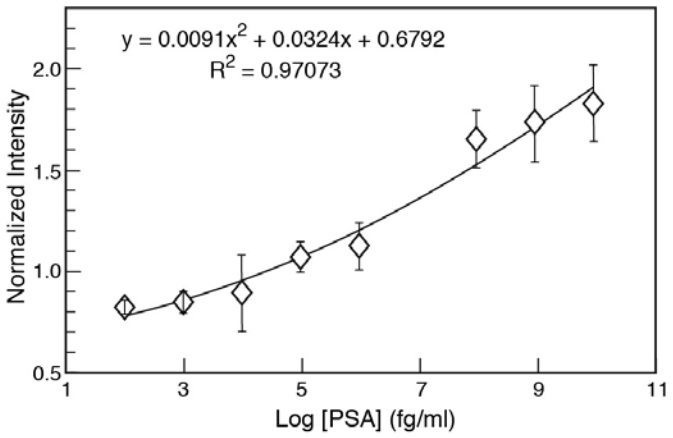

Figure 10. Plot of log PSA concentration (fg/ml) versus integrated intensity at Raman peak located at 1338 cm^{-1} normalized by peak intensity at 632 cm^{-1}. Concentrations ranged from 100fg/ml to 1 ng/ml.

The large absorbance near the NIR laser excitation wavelength is responsible for the increased resonance and subsequent signal sensitivity of these Raman labels when excited at 785 nm, as opposed to 633 nm as in earlier studies.[5] Excitation at 785 nm also has other advantages. Biological samples, such as antibodies and antigens, show reduced autofluorescence and photo-degradation when excited in the NIR region. Additionally, some cases have been documented where the chemical component of SERS enhancement can be exaggerated using NIR excitation. Gold colloids have also been shown to achieve strong resonances in this region, resulting in increased electromagnetic enhancement as well.[25] Some materials display Raman enhancement specific to 785 nm excitation. These peaks are thought to be due to the selective excitation of different structural units at material boundaries.[26] Here, the excitation is most likely occurring at the DSNB labels when an interface between AuNPs is within a reactive distance. Michaels et al.[27] found that significant SERS enhancement occurs at the junction of two or more nanoparticles. Aggregates with multiple particles yielded large enhancements due to a large electromagnetic field at these interfaces.

4. CONCLUSION

SERS spectra of rhodamine 6G with freshly prepared Au nanoparticles excited with 785 nm laser show that it is possible to detect R6G down to 10^{-8} M. Using nitrocellulose as substrate and DSNB-labeled AuNPs in the dot blot configuration, we have shown that protein A and PSA can be detected down to 100 fg/ml. The specificity for each of these assays is imparted by the antibodies' affinity to its antigen. This assay format could be extended for use with any biological molecule, given the choice of the appropriate antibody. Reporters made from smaller AuNPs with the ability to form large aggregates gave a significantly greater SERS signal with 785 nm excitation. This is believed to be due to the increased number of active SERS sites at junctions between AuNPs within the aggregates as well as a greater SERS enhancement achieved at this excitation wavelength due to aggregated AuNPs' shifted plasmon absorbance to near infrared region. It is anticipated that the lower detection limits for biomarkers such as PSA achieved in the present study will allow screening of condition such as prostate cancer with smaller volumes of clinical samples and at earlier stages of disease progression.

ACKNOWLEDGMENTS

This work is supported in part by the Army Research Laboratory under cooperative agreement W911MF-07-2-0002, and U.S. Army Medical Research and Materiel Command contract W81XWH-10-2-0191. The authors would like to thank Nancy Hulbirt and May Izumi for their valuable help with figures and editing, respectively. This is SOEST contribution no. 8082 and HIGP contribution no. 1880.

REFERENCES

[1] Kambhampati, P., Child, C. M., Foster, M. C. and Campion, A., "On the chemical mechanism of surface enhanced Raman scattering: Experiment and theory," J Chem Phys 108, 5013-5026 (1998).

[2] Porter, M. D., Lipert, R. J., Siperko, L. M., Wang, G., and Narayanana, R., "SERS as a bioassay platform: fundamentals, design, and applications," Chem Soc Rev 37, 1001-1011 (2008).

[3] Hering, K., Cialla, D., Ackermann, K., Dorfer, T., Moller, R., Schneidewind, H., Mattheis, R., Fritzsche, W., Rosch, P., and Popp, J., "SERS: a versatile tool in chemical and biochemical diagnostics," Anal Bioanal Chem 390, 113-124 (2008).

[4] Chen, J. W., Jiang, J. H., Gao, X., Gong, J. L., Shen, G. L., and Yu, R. Q., "Gold-aggregated, dye-embedded, polymer-protected nanoparticles (GDPNs): A new type of tags for detection with SERS," Colloid Surface A 294, 80-85 (2007).

[5] Grubisha, D. S., Lipert, R. J., Park, H. Y., Driskell, J. and Porter, M. D. "Femtomolar detection of prostate-specific antigen: an immunoassay based on surface-enhanced Raman scattering and immunogold labels," Anal Chem 75, 5936-5943 (2003)

[6] Jemal, A., Siegel, R., Ward, E., Murray, T., Xu, J., and Thun, M. J., "Cancer statistics, 2007," CA Cancer J Clin 57, 43-66 (2007).

[7] www.cancer.gov/cancertopics/factsheet/Detection/early-prostate

[8] Yu, H., Diamandis, E. P., Prestigiacomo, A. F. and Stamey, T. A., "Ultrasensitive assay of prostate-specific antigen used for early detection of prostate cancer relapse and estimation of tumor-doubling time after radical prostatectomy," Clin Chem 41, 430-434 (1995).

[9] Morcol T. and Subramanian, A., "A red-dot-blot protein assay technique in the low nanogram range," Anal Biochem 270, 75-82 (1999).

[10] Nezlin, R., "A quantitative approach to the determination of antigen in immune complexes," J Immun Methods 237, 1-17 (2000).

[11] Noya, O. and de Noya, B. A., "The multiple antigen blot assay (MABA): a simple immunoenzymatic technique for simultaneous screening of multiple antigens," Immun Letts 63, 53-56 (1998).

[12] Nakamura, K., Tanaka, T., Kuwahara, A. and Takeo, K., "Microassay for Proteins on Nitrocellulose Filter Using Protein Dye-Staining Procedure," Anal Biochem 148, 311-319 (1985).

[13] Lin, C. C., Yang, Y. M., Chen, Y. F., Yang, T. S. and Chang, H. C., "A new protein A assay based on Raman reporter labeled immunogold nanoparticles," Biosens Bioelectron 24 (2), (2008).

[14] Sinha, P., Sengupta, J. and Ray, P. K., "Functional mimicry of protein A of Staphylococcus aureus by a proteolytically cleaved fragment," Biochem Biophys Res Comm 260, 111-116 (1999).

[15] Ray, P. K., Bandyopadhyay, S., Dohadwala, M., Canchanapan, P. and Mobini, J., "Antitumor-Activity with Nontoxic Doses of Protein-A," Cancer Immunol Immun 18, 29-34 (1984)

[16] Slot, J. W. and Geuze, H. J., "Sizing of protein A-colloidal gold probes for immunoelectron microscopy," J Cell Biol 90, 533-536 (1981).

[17] Saraiva, S. A. and de Oliveira, J. F., "Control of particle size in the preparation of colloidal gold," J. Dispersion Sci. Technol. 23, 93–123 (2002).

[18] Lazarides, A. A. and Schatz, G. C., "DNA-linked metal nanosphere materials: Structural basis for the optical properties," J Phys Chem B 104, 2987-2993 (2000).

[19] Hildebrandt, P. and Stockburger, M., "Surface-Enhanced Resonance Raman-Spectroscopy of Rhodamine-6G Adsorbed on Colloidal Silver," J Phys Chem 88, 5935-44 (1984).

[20] Patungwasa, W. and Hodak, J. H., "pH tunable morphology of the gold nanoparticles produced by citrate reduction," Mat Chem Phys 108, 45–54 (2008).

[21] Kwon, K., Lee, Y. K. Y., Lee, W., Kim, M., Heo, J., Ahn, S. J. and Han, S. W., "Controlled synthesis of icosahedral gold nanoparticles and their surface-enhanced Raman scattering property," J Phys Chem C 111, 1161–1165 (2007)

[22] Schwartzberg, A. M., Grant, C. D., Wolcott, A., Talley, C. E., Huser, T. R., Bogomolni, R.and Zhang, J. Z., "Unique gold nanoparticle aggregates as a highly active surface-enhanced Raman scattering substrate," J Phys Chem B 108, 19191–19197 (2004).

[23] Nash, A. F. and Melezinek, I., "The role of prostate specific antigen measurement in the detection and management of prostate cancer," Endocr Relat Cancer 7, 37-51(2000).

[24] Vassilikos, E. J. K., Yu, H., Trachtenberg, J., Nam, R. K., Narod, S. A., Bromberg, I. L., and Diamandis, E. P. "Relapse and cure rates of prostate cancer patients after radical prostatectomy and 5 years of follow-up," Clin Biochem 33, 115- 123 (2000).
[25] Kneipp, K., Dasari, R. R., and Wang, Y., "Near-Infrared Surface-Enhanced Raman-Scattering (Nir Sers) on Colloidal Silver and Gold," Appl Spectrosc 48, 951-957(1994).
[26] May, P. W., Smith, J. A. and Rosser, K. N., "785 nm Raman spectroscopy of CVD diamond films," Diam Relat Mater 17, 199-203 (2008).
[27] Michaels, A. M., Jiang, J. and Brus, L., "Ag nanocrystal junctions as the site for surface-enhanced Raman scattering of single Rhodamine 6G molecules," J Phys Chem B 104, 11965–11971 (2000).

Appendix V: Reprint Proceedings SPIE, 8367, 836705/1-836705/10 (2012)

In vitro quantitation of human femoral artery atherosclerosis using near-infrared Raman spectroscopy

Ava C. Dykes[a], Pavlos Anastasiadis[b, c], John S. Allen III[c], and Shiv K. Sharma[a]

[a] University of Hawaii, Hawaii Institute for Geophysics and Planetology, 1680 East-West Rd., POST #602, Honolulu, Hawaii 96822

[b] Department of Molecular Biosciences & Bioengineering, University of Hawaii at Manoa, Honolulu, HI 96822

[c] Department of Mechanical Engineering, University of Hawaii at Manoa, 2540 Dole St., Holmes Hall 302, Honolulu, HI 96822

ABSTRACT

Near-infrared Raman spectroscopy has been used *in vitro* to identify calcified atherosclerotic plaques in human femoral arteries. Raman techniques allow for the identification of these plaques in a nondestructive manner, which may allow for the diagnosis of coronary artery disease in cardiac patients in the future. As Raman spectroscopy also reveals chemical information about the composition of the arteries, it can also be used as a prognostic tool. The *in vivo* detection of atherosclerotic plaques at risk for rupture in cardiac patients will enhance treatment methods while improving clinical outcomes for these procedures. Raman spectra were excited by an Invictus 785-nm NIR laser and measured with a fiber-coupled micro-Raman RXN system (Kaiser Optical Systems, Inc., Ann Arbor, MI) equipped with a 785 nm CW laser and CCD detector. Chemical mapping of arteries obtained *post mortem* allowed for the discrete location of atherosclerotic plaques. Raman peaks at 961 and 1073 cm^{-1} reveal the presence of calcium hydroxyapatite and carbonate apatite, which are known to be present in calcified plaques. By mapping the locations of these peaks the boundaries of the plaques can be precisely determined. Areas of varying degrees of calcification were also identified. Because this can be useful in determining the degree of plaque calcification and vessel stenosis, this may have a significant impact on the clinical treatment of atherosclerotic plaques in the future.

Keywords: atherosclerosis, atherosclerotic plaque, plaque calcification, near-infrared Raman spectroscopy, chemical mapping, SERS

1. INTRODUCTION

Atherosclerosis is a systemic disease in which fatty deposits, inflammation, cells, and scar tissue build up within artery walls. In advanced lesions these deposits accumulate, followed by the formation of calcium containing crystals. This ultimately leads to calcification of the artery wall.[1] Atherosclerosis now accounts for nearly three-fourths of all deaths from cardiovascular disease and is the underlying cause of the majority of clinical cardiovascular events such as heart attack and stroke.[2] Both coronary artery disease (CAD) and peripheral artery disease (PAD) are clinical manifestations of atherosclerosis. However, patients diagnosed with atherosclerosis tend to develop the disease in different types of arteries. Approximately 60% of patients with severe PAD requiring surgery were found to have significant CAD in at least one vessel.[3] In fact, PAD is known to be a marker for systemic atherosclerosis.[2] For this reason, it is important to study atherosclerosis in vessels of the extremities. The femoral artery is of particular interest because 72% of all occlusions occurring in the leg originate in the femoral artery within the adductor canal.[4]

In the majority of cases, atherosclerosis is not detected until it becomes symptomatic, such as when significant stenosis or occlusion occurs. However, asymptomatic or noncritical stenoses are also clinically relevant. The rupture of nonocclusive plaques followed by rapid plaque enlargement is the most important mechanism for acute coronary syndromes such as myocardial infarction and crescendo angina.[5] Recent studies support the theory that plaque composition rather than size or volume determines whether a lesion will rupture and could lead to a cardiac event.[6]

Smart Biomedical and Physiological Sensor Technology IX, edited by Brian M. Cullum, Eric S. McLamore,
Proc. of SPIE Vol. 8367, 836705 · © 2012 SPIE · CCC code: 1605-7422/12/$18 · doi: 10.1117/12.918520

Current technology offers only limited information about plaque composition. Intravascular ultrasound yields mainly morphological information. Magnetic resonance imaging (MRI) can detect large lipid pools and calcifications but cannot quantify the chemical composition of these areas. Directional coronary atherectomy provides histological information but is a destructive technique and only detects advanced lesions.[6] Autofluorescence showed some promise as a laser angioplasty guidance system due to the inherent fluorescence of vessel wall and atherosclerotic plaque constituents, but this method offers little biochemical information.[7] For these reasons Raman spectroscopy has become an ideal candidate for the detection of early atherosclerosis. Raman techniques are noninvasive, nondestructive, and can reveal the chemical composition of the target tissue. The use of near-infrared Raman spectroscopy eliminates interference from inherent autofluorescence.

Normal Raman scattering occurs when monochromatic light interacts with molecules in a sample. This interaction causes the energy of laser photons to be shifted up or down, known as Raman shifts. The Raman shifts give information about the vibrational modes of the molecules and thus provide Raman "fingerprints" for identification of various biological molecules in the sample. When a spectrometer is coupled with a microscope, micro-Raman techniques offer the advantage of reduced sample volume ($<1\ \mu m^3$) and superior spatial resolution ($\sim 1 \mu m$).[8]

A variation of micro-Raman scattering that has proven valuable in the study of biological samples is surface-enhanced Raman scattering (SERS). SERS occurs when Raman scattering takes place within a sample that is in the presence of a roughened metal surface or metal nanoparticles, such as gold or silver. An enhanced electromagnetic field produced at the surface of the metal allows for the excitation of electrons into an extended surface electronic excited state, called a surface plasmon resonance. [9] With a typical signal enhancement of 10^6 to 10^{14} over that of traditional Raman detection systems, SERS offers specificity and sensitivity comparable to that of fluorescence techniques with added advantages. First, Raman bands are 10-100 times narrower than those of fluorescence. This reduces the likelihood of spectral overlap when multiple labels are used. Second, the SERS excitation wavelength is dependent on the chemical and physical properties of the enhancing substrate, not the target label. This enables the use of a single excitation wavelength. And lastly, Raman emissions are less susceptible to photobleaching than fluorescence. This allows for the use of an extended excitation period that may lead to lower detection limits. [10]

2. METHODOLOGY

2.1 Human Artery Samples

Human femoral arteries were obtained *post mortem* from an individual whose cause of death was a cardiac event. Artery segments were frozen at -30°C until sectioning. Ten micron sections were captured on 1"x3" slides cut from commercially available polished aluminum sheets with a thickness of 0.5 mm (Anomet, Inc., Ontario, Canada). Sections mounted on aluminum slides were stored at -80°C. Slides were warmed to room temperature before examination by Raman spectroscopy.

Artery sections interrogated by SERS immunohistochemistry required further preparation. Ten micron sections of human femoral artery mounted on aluminum slides were fixed and permeated by exposure to ice-cold methanol for 5 minutes. After rinsing three times with phosphate-buffered saline (PBS), arteries were blocked using 5% bovine serum albumin (BSA) in PBS for 1 hour. Sections were again rinsed three times with PBS before treatment with an antibody-DSNB-AuNP reporter as described below. Arteries were next exposed to either anti-von Willebrand factor (vWF)-DSNB-AuNP or anti-Ki67-DSNB-AuNP reporters for 1 hour at room temperature. The slides were then rinsed three times in PBS and allowed to air dry before study.

2.2 SERS Probes

Gold colloids (gold nanoparticles or AuNPs) were made by adding 1 ml of 1% hydrogen tetrachloroaurate (III) ($HAuCl_4$) to 100 ml of distilled water, followed by 2 ml of 1% sodium citrate tribasic dihydrate ($Na_3C_6H_5O_7$). Approximately 1 ml of 0.1M K_2CO_3 was added to adjust the pH to 7.0 [11]. The solution was then heated under reflux for 20 to 30 minutes, until the color turned deep purple. Evaluation by photon correlation spectroscopy performed on gold colloids prepared in this manner revealed particle size to be approximately 20 nm. The concentration of AuNPs in a typical solution was calculated to be 9.23×10^{11} particles/ml.

Synthesis of 5, 5′-dithiobis (succinimidyl-2-nitrobenzoate) was carried out as previously described.[12] Briefly, 0.50 g of 5, 5′-dithiobis (2-nitrobenzoic acid) (DNBA), 0.52 g of 1, 3-dicyclohexylcarbodiimide (DCCD), and 0.29 g of *N*-hydroxysuccinimide (NHS) were sequentially added to 50 ml tetrahydrofuran in a 500 ml round-bottom flask equipped with a drying tube. After stirring for 24 hours at room temperature, the solution was filtered, then rotoevaporated to remove the solvent. The product was recrystallized as a yellow powder with acetone/hexane solvent.

DSNB-labeled SERS reporters were constructed as previously described.[13] In brief, reporters were made by adding 100 µl of 2.5mM DSNB in acetonitrile to 1 ml of unconjugated gold sol. The resulting reaction was allowed to proceed for 4 to 8 hours. The mixture was then centrifuged at 10,000 *g* for 7 minutes. The clear supernatant was discarded and the loose sediment resuspended in 1 ml borate buffer (2mM, pH 9). Next, 35 µg of detection antibody was added. The detection antibodies used here included rabbit polyclonals to either von Willebrand Factor (vWF) or Ki67 (Abcam, Inc. Cambridge, MA). This mixture was incubated at room temperature for 1 hour. After a second centrifugation and removal of the supernatant, the precipitate was resuspended in 1 ml of 2mM Tris buffer (pH 7.6) with 1% BSA.

Figure 1 demonstrates the basic reaction between DSNB and a single gold nanoparticle. The interaction of DSNB with the gold surface results in AuNP coated with a thiolate of DSNB. The intermediate species formed is a Raman-reporter-labeled AuNP containing a reactive group, R ($C_5H_5NO_3$). This Raman reporter molecule can then react with the primary amine of an antibody by the formation of an amide linkage,[12] creating a bifunctional Raman reporter.

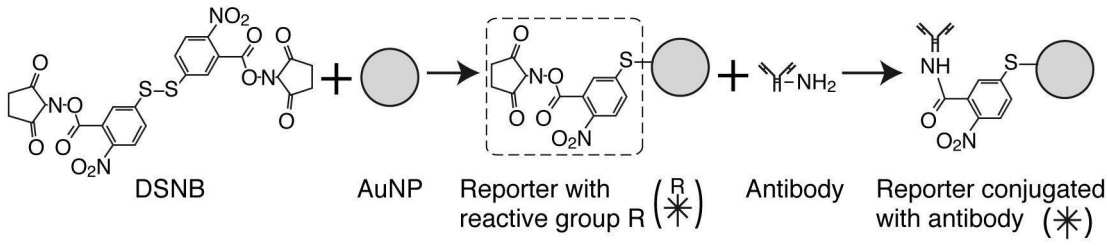

Figure 1. Conjugation chemistry of DSNB molecule with AuNPs. Exposure of DSNB to the gold surface yields an AuNP coated with the thiolate of DSNB. The thiolate contains a reactive group that then forms an amide linkage with the primary amine of an antibody.

2.3 Micro-Raman spectroscopy

All Raman spectra were excited by the Invictus 785-nm NIR laser and measured with a fiber-coupled micro-Raman RXN system (Kaiser Optical Systems, Inc., Arbor, MI) equipped with a 50 micron slit. The micro-Raman system uses a 785 nm CW laser and CCD detector. A 50× objective that produced a 5 µm laser spot size on the sample was used for all measurements. The Rayleigh scattered laser light at 785 nm was rejected by utilizing a 785 nm holographic notch filter (Kaiser Optical System, Inc.). The cosmic rays were removed by the software provided by Kaiser optical system, which measures the spectra twice and deletes the random peaks due to cosmic rays. The spectra were collected with 10 mW of laser power at the sample and 120 s of integration time.

Chemical mapping was used to evaluate human femoral arteries. A 10x10 matrix of points was selected for Raman sampling for a total of 100 spectra from each area. Areas containing calcified plaques were identified by mapping the intensity of peaks 961 and 1073cm^{-1}. Areas containing high amounts of cholesterol were identified by mapping the intensity of the peak at 1442cm^{-1}.

SERS spectra were also obtained with the fiber-coupled micro-Raman RXN system. These spectra were collected with 10 mW of laser power at the sample and 60 s of integration time.

3. RESULTS AND DISCUSSION

Representative Raman spectra are shown in Figures 2 and 3. Spectra from sections of artery containing calcified plaques are known to be two to five fold higher in intensity than normal areas.[1] Peaks associated with cholesterol also have higher intensity, reflecting a higher concentration of the material in these areas. The peaks at 1442cm^{-1} and the area from 2800 to 3000cm^{-1} are most obviously affected. The presence of peaks that are unique to the calcified plaque areas is also notable. Strong peaks at 961 and 1073 cm^{-1} are due to phosphate and carbonate symmetric stretching in calcium hydroxyapatite and carbonate apatite, respectively.

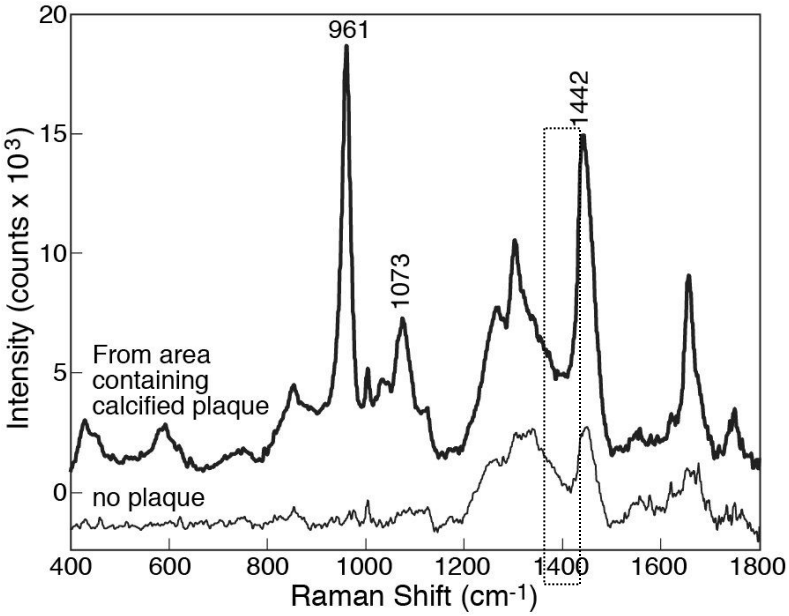

Figure 2. Representative spectra from human femoral artery. Major peaks are noted: 961cm^{-1}, phosphate from calcium hydroxyapatite; 1073cm^{-1}, carbonate from carbonate apatite; 1442cm^{-1}, cholesterol and cholesterol esters.

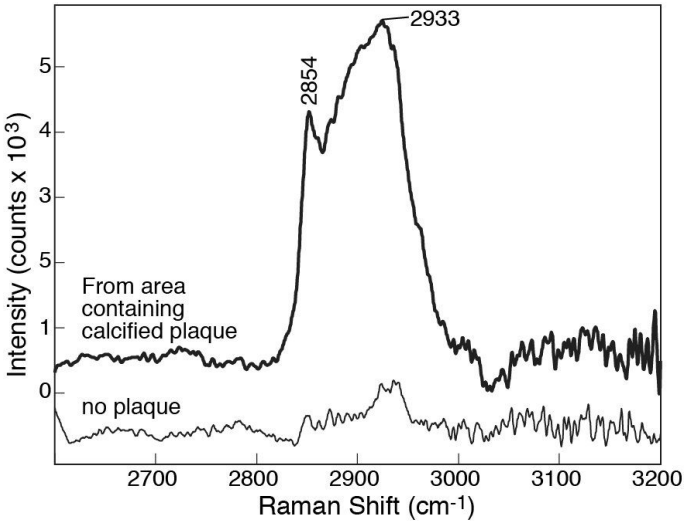

Figure 3. Represenative spectra from human femoral artery. The area from 2800 to 3000cm^{-1} represents peaks associated with cholesterol and its esters.

Other noted Raman peaks are listed in Table 1. The Raman lines associated with the aromatic ring in the amino acid phenylalanine are located at 1004 and 1037 cm^{-1}.[14] β-carotene is found in miniscule amounts in human arteries, however, it is a strong Raman scatterer and contributes to the artery spectrum by presenting a peak at 1130 cm^{-1} resulting from C-C and C=C stretching mode. [1, 6] Amide III vibrations are evidenced by peaks at 1267 and 1303 cm^{-1}, while amide I vibrations are detected at 1656 cm^{-1}. [1, 14, 15] A dominant band appears at 1442 cm^{-1}; this peak is the result of CH_2 bending from cholesterol and its esters. [1, 15] A peak located at 1749 cm^{-1} results from the C=O found in palmitic triglyceride. [16]

Table 1. Tentative assignment and Raman peak positions observed with 785nm excitation.

Frequency (cm^{-1})	**Assignment**
961	Phosphate symmetric stretching due to calcium hydroxyapatite [1, 15]
1004	Phenylalanine aromatic ring [14]
1037	Phenylalanine aromatic ring [14]
1073	carbonate symmetric stretching due to carbonate apatites [1, 15]
1130	C-C, C=C stretch mode from β-carotene accumulation [1]
1267	Amide III vibration [1]
1303	Amide III vibration, δ(CH) [14]
1442	CH_2 bending from cholesterol and cholesterol esters [1, 15]
1656	Amide I vibration [15]
1749	C=O from palmitic triglyceride [16]

Chemical mapping based on prominent Raman peaks was also used to evaluate human femoral arteries. A 10x10 matrix of points was selected for Raman sampling for a total of 100 spectra from each area. Typical results are shown in Figs. 4, 5, and 6. Areas containing calcified plaques were identified by mapping the intensity of peaks 961 and 1073cm^{-1}. Areas containing high amounts of cholesterol were identified by mapping the intensity of the peak at 1442 cm^{-1}.

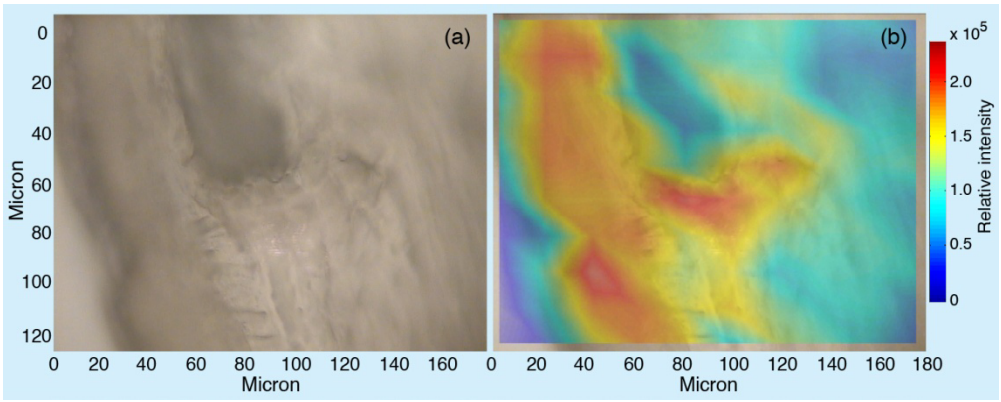

Figure 4. (Left) White light image of 50X area of artery. (Right) Chemical mapping of peak 961cm^{-1} overlay on white light image. Red areas indicate high peak intensity while blue areas are low intensity.

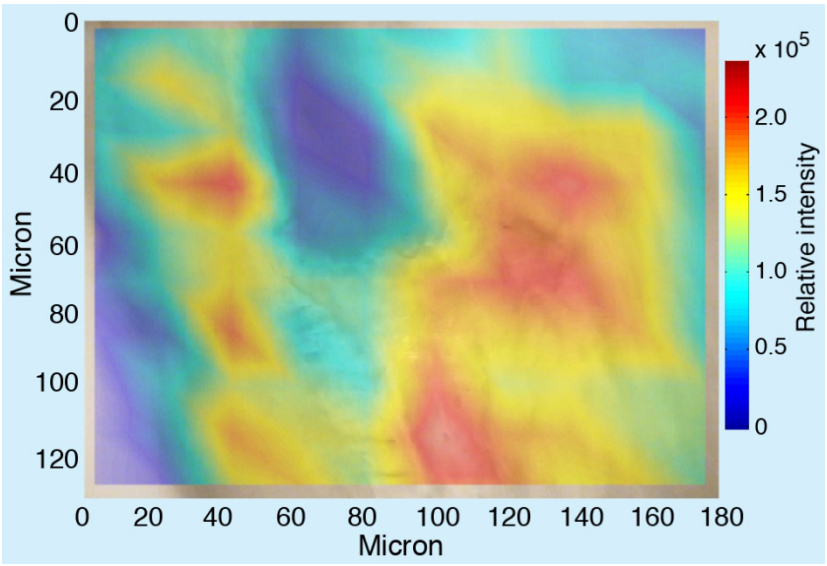

Figure 5. Chemical mapping of peak 1073cm^{-1} overlay on white light image. This peak represents the presence of carbonate in carbonate apatite in calcified plaques. Red areas indicate high peak intensity while blue areas are low intensity.

Figure 4 shows a composite white light image and a chemical Raman map of an area of femoral artery. This Raman map was generated using HoloMap software (Kaiser Optical System, Inc.) by mapping the intensity of the peak located at 961cm^{-1}. The areas of high intensity represent where high concentrations of phosphate from calcium hydroxyapatite are located within the vessel wall. Similarly, Fig. 5 maps the Raman intensity of the peak at 1073cm^{-1}, which is indicative of carbonate present in carbonate apatite. Both calcium hydroxyapatite and carbonate apatite are known constituents of calcified atherosclerotic plaques.

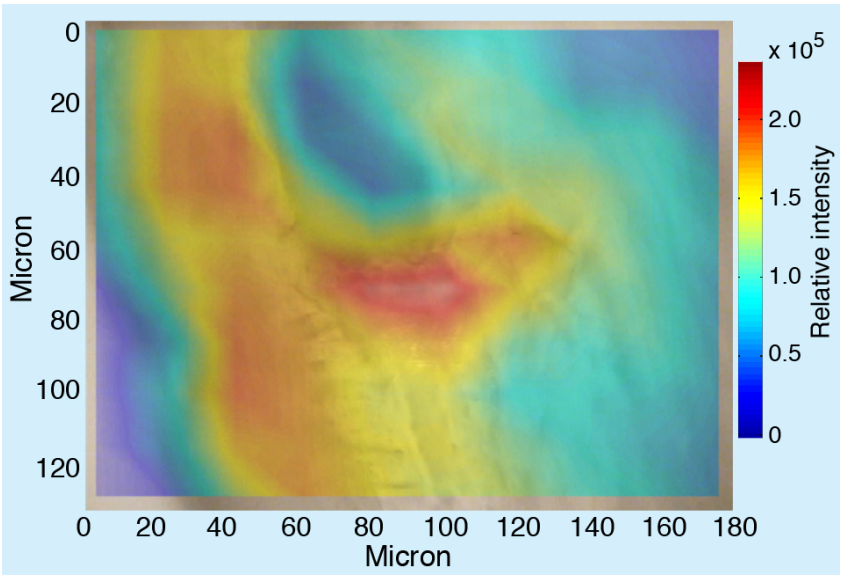

Figure 6. Chemical mapping of peak 1442cm^{-1} overlay on white light image. This peak represents the presence of cholesterol accumulations and may be sites of early plaque formations. Red areas indicate high peak intensity while blue areas are low intensity.

Figure 6 shows a chemical map based on the intensity of the Raman peak located at 1442cm^{-1}. This peak is associated with the CH_2 deformation mode of cholesterol and its esters. Cholesterol accumulates early in the atherosclerotic process. However, these cholesterol deposits are part of a calcified plaque. Figures 4, 5, and 6 are maps of the same area created using different Raman shifts. Examination of the maps reveals that calcium hydroxyapatite, carbonate apatite, and cholesterol all colocalize within this site to form a large area of atherosclerotic plaque.

SERS technology can be applied to the study of atherosclerotic arteries through the use of immunohistochemistry techniques. Ten micron sections of human femoral artery mounted on aluminum slides were fixed and permeated by exposure to ice-cold methanol for 5 minutes. After rinsing three times with phosphate-buffered saline (PBS), arteries were blocked using 5% BSA in PBS for 1 hour. Sections were again rinsed three times with PBS before treatment with an antibody- DSNB-AuNP reporter as described above. Arteries were exposed to either anti-vWF-DSNB-AuNP or anti-Ki67-DSNB-AuNP reporters for 1 hour at room temperature. Slides were then rinsed three times in PBS and allowed to air dry before examination by Raman spectroscopy.

To understand the distribution of these proteins in arterial tissue, chemical mapping of areas of the artery was performed using antibody-labeled SERS reporters. A 10x10 matrix of points was selected for Raman sampling for a total of 100 spectra from each area. A typical spectrum is shown in Fig. 7. Prominent peaks indicate the presence of a DSNB SERS reporter. These peaks include 851 cm^{-1} (nitro scissoring vibration), 1076 cm^{-1} (succinimidyl N-C-O stretch overlapping with aromatic ring modes), 1333 cm^{-1} (symmetric nitro stretch), and 1558 cm^{-1} (aromatic ring mode (8a)). The primary band located at 1333 cm^{-1} was used for chemical mapping. Areas of high intensity (in red) represent areas where high concentrations of the target antigen have been recognized by the antibody-DSNB-AuNP complex. Representative chemical SERS map results are shown in Fig. 8.

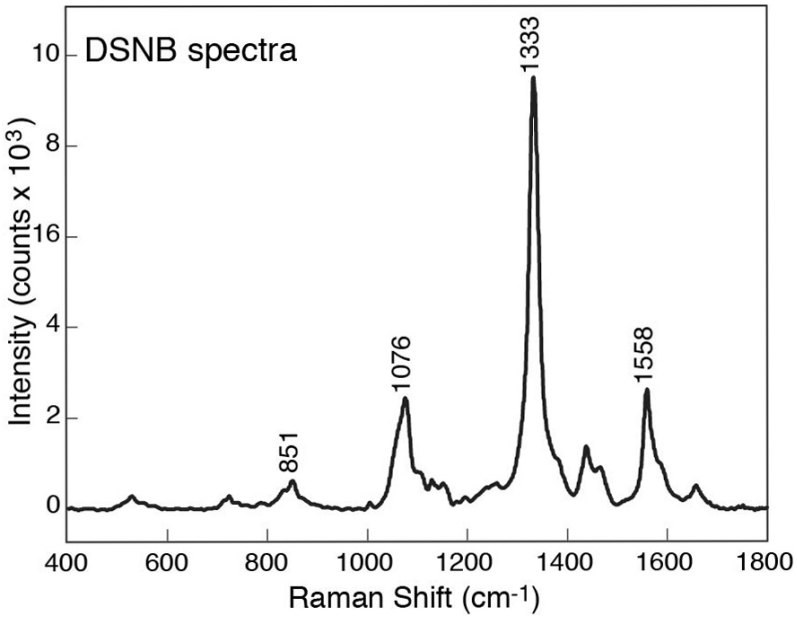

Figure 7. Representative anti-vWF-DSNB-AuNP reporter spectrum. Prominent DSNB peaks are labeled for clarity: 851 cm^{-1} (nitro scissoring vibration): 1076 cm^{-1} (succinimidyl N-C-O stretch overlapping with aromatic ring modes): 1333 cm^{-1} (symmetric nitro stretch): and 1558 cm^{-1} (aromatic ring mode (8a)). All SERS spectra were collected with the micro-*Raman RXN system* (Kaiser Optical Systems, Inc., Arbor, MI) using 10 mW of laser power and 60 s of integration time.

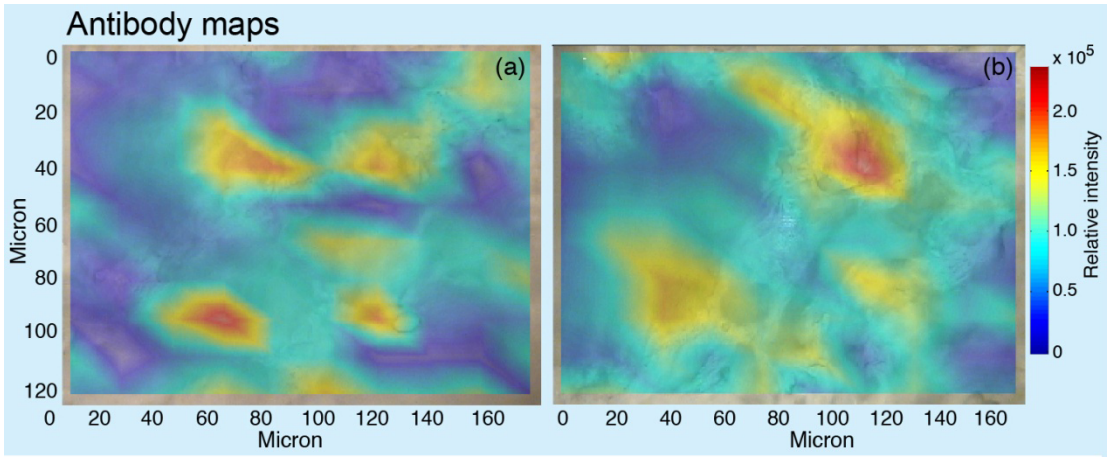

Figure 8. SERS detection of labeled antigens in human femoral arteries. (left) Distribution of anti-Ki67-DSNB-AuNP reporter in femoral artery tissue. (right) Distribution of anti-vWF-DSNB-AuNP reporter. Red indicates areas of high intensity while blue indicates areas of low intensity.

Chemical mapping using SERS immunohistochemistry has several advantages over other antigen detection techniques. First, SERS sensitivity has been shown to be superior to other readout methods. [12, 13, 17] SERS-based immunoassays had limits of detection (LODs) 10^2 to 10^3 lower than conventional fluorescence-based assays. [12, 13] Secondly, autofluorescence introduces a huge obstacle to immunodetection of antigens with fluorescence reporters. This autofluorescence arises from the complex molecules that comprise the walls of the vasculature. Collagen, elastin, and cholesterol exhibit autofluorescence over a wide spectrum of wavelengths.[18] Elastin in particular contains several fluorescing molecules, including a tricarboxylic amino acid with a pyridinium ring. Collagen contains a similar fluorophore.[19] These connective tissues have major fluorescent emission bands between 400 and 460nm, resulting in

blue autofluorescence. [20, 21] Cholesterol has yellow autofluorescence (570-590nm) while cholesterol esters appear orange (585-620nm).[21] All of these occur at wavelengths less than Raman excitation at 785nm and so these fluorescence bands do not interfere with this type of histochemical analysis of arterial tissue.

Anti-Ki67-DSNB-AuNP reporters revealed the distribution of the Ki67 antigen to be aggregated in discrete areas. Ki67 is a proliferation marker and is expected to be found in tissues exhibiting rapid growth. This protein is found in areas where there is proliferation of macrophages, which is a key step in the progression and destabilization of atherosclerotic plaques. [21] Anti-vWF-DSNB-AuNP reporters also found vWF to be allocated to concentrated areas of the artery. vWF is a glycoprotein that promotes the binding of platelets to sites of injury at vessel walls, an initial step in the formation of some types of atherosclerotic plaques. [22] Both Ki67 and vWF are markers for early stage atherosclerosis. Thus these SERS-based reporters can identify areas that will be vulnerable to plaque formation at later stages of development.

4. CONCLUSIONS

Near-infrared Raman spectroscopy has been used to identify areas of atherosclerotic plaque in human femoral arteries. Chemical Raman mapping was used to delineate areas of calcified plaque. Raman peaks at 961, 1073, and 1442 cm^{-1} are known to be associated with plaque constituents and these peak positions were employed to identify areas containing calcium hydroxyapatite, carbonate apatite, and cholesterol, respectively. SERS immunohistochemistry was also used in combination with chemical mapping to identify areas with early atherosclerotic plaque formation. Antibodies to early atherosclerotic markers were used to construct SERS-based reporters. By mapping the location of the DSNB reporter used, the localization of these proteins was revealed. Anti-Ki67-DSNB-AuNP and anti-vWF-DSNB-AuNP reporters showed discrete areas of early plaque formation in femoral artery sections.

ACKNOWLEDGMENTS

This work was supported in part by the U.S. Army Medical Research and Materiel Command contract W81XWH-10-2-0191. The authors would like to thank Nancy Hulbirt and May Izumi for their valuable help with figures and editing, respectively. This is SOEST contribution no. 8708 and HIGP contribution no. 1982.

REFERENCES

[1] L. Silveira, S. Sathaiah, R. A. Zangaro *et al.*, "Correlation between near-infrared Raman spectroscopy and the histopathological analysis of atherosclerosis in human coronary arteries," Laser Surg Med, 30(4), 290-297 (2002).

[2] D. Lloyd-Jones, "Heart Disease and Stroke Statistics-2009 Update: A Report from the American Heart Association Statistics Committee and Stroke Statistics Subcommittee (vol. 119, pg e21, 2009)," Circulation, 122(1), E11-E11 (2010).

[3] A. Cassar, D. Poldermans, C. S. Rihal *et al.*, "The management of combined coronary artery disease and peripheral vascular disease," European Heart J., 31(13), 1565-U30 (2010).

[4] P. J. W. Wensing, L. Meiss, W. P. T. M. Mali *et al.*, "Early atherosclerotic lesions spiraling through the femoral artery," Arteriosclerosis Thrombosis and Vascular Biology, 18(10), 1554-1558 (1998).

[5] J. P. Salenius, J. F. Brennan, A. Miller *et al.*, "Biochemical composition of human peripheral arteries examined with near-infrared Raman spectroscopy," Journal of Vascular Surgery, 27(4), 710-719 (1998).

[6] T. J. Romer, J. F. Brennan, M. Fitzmaurice *et al.*, "Histopathology of human coronary atherosclerosis by quantifying its chemical composition with Raman spectroscopy," Circulation, 97(9), 878-885 (1998).

[7] G. V. Nogueira, L. Silveira, A. A. Martin *et al.*, "Raman spectroscopy study of atherosclerosis in human carotid artery," J. Biomed. Opt. 10(3), 031117 (2005).

[8] R. J. Swain, and M. M. Stevens, "Raman microspectroscopy for non-invasive biochemical analysis of single cells," Biochem. Soc. Trans., 35, 544-549 (2007).

[9] A. Campion, and P. Kambhampati, "Surface-enhanced Raman scattering," Chem Soc Rev, 27(4), 241-250 (1998).
[10] D. S. Grubisha, R. J. Lipert, H. Y. Park *et al.*, "Femtomolar detection of prostate-specific antigen: An immunoassay based on surface-enhanced Raman scattering and immunogold labels," Anal Chem, 75(21), 5936-5943 (2003).
[11] J. W. Slot, and H. J. Geuze, "Sizing of protein A-colloidal gold probes for immunoelectron microscopy," J Cell Biol, 90(2), 533-6 (1981).
[12] D. S. Grubisha, R. J. Lipert, H. Y. Park *et al.*, "Femtomolar detection of prostate-specific antigen: an immunoassay based on surface-enhanced Raman scattering and immunogold labels," Anal Chem, 75(21), 5936-43 (2003).
[13] A. C. Dykes, L. Kamemoto, A. K. Misra *et al.*, "Nitrocellulose-based SERS immunosensor for detection of biological molecules," Proc. SPIE, 8025, (2011).
[14] P. V. Zinin, A. Misra, L. Kamemoto *et al.*, "Visible, near-infrared, and ultraviolet laser-excited Raman spectroscopy of the monocytes/macrophages (U937) cells," J. Raman Spectrosc., 41(3), 268-274 (2010).
[15] L. Silveira, G. V. Nogueira, A. A. Martin *et al.*, "Raman spectroscopy study of atherosclerosis in human carotid artery," J. Biomed. Opt. 10(3), (2005).
[16] R. Manoharan, J. J. Baraga, M. S. Feld *et al.*, "Quantitative histochemical analysis of human artery using Raman spectroscopy," Journal of Photochemistry and Photobiology B-Biology, 16(2), 211-233 (1992).
[17] K. Kneipp, H. Kneipp, and H. G. Bohr, "Single-molecule SERS spectroscopy," Surface-Enhanced Raman Scattering: Physics and Applications, 103, 261-277 (2006).
[18] K. Kingsley, K. Carroll, J. L. Huff *et al.*, "Photobleaching of arterial autofluorescence for immunofluorescence applications," Biotechniques, 30(4), 794-797 (2001).
[19] Z. Deyl, K. Macek, M. Adam *et al.*, "Studies on the chemical nature of elastin fluorescence," Bioch. Biophys. Acta, 625, 248-254 (1980).
[20] H. W. Wang, J. Willis, M. I. F. Canto *et al.*, "Quantitative laser scanning confocal autofluorescence microscopy of normal, premalignant, and malignant colonic tissues," IEEE Trans. on Biomed. Eng., 46(10), 1246-1252 (1999).
[21] Y. Uchida, Y. Uchida, S. Kawai *et al.*, "Detection of Vulnerable Coronary Plaques by Color Fluorescent Angioscopy," JACC-Cardiovascular Imaging, 3(4), 398-408 (2010).
[22] J. E. Sadler, "Biochemistry and genetics of von Willebrand factor," Ann. Rev. Biochem., 67, 395-424 (1998).